DOKUZ EYLÜL UNIVERSITY

GRADUATE SCHOOL OF NATURAL AND APPLIED SCIENCES

RELATION BETWEEN INDUCED SEISMICITY AND GEOTHERMAL SYSTEMS: A CASE STUDY FROM THE GEDIZ GRABEN, WESTERN ANATOLIA, TURKEY

by

Hüseyin UYTUN

October, 2021

İZMİR

RELATION BETWEEN INDUCED SEISMICITY AND GEOTHERMAL SYSTEMS: A CASE STUDY FROM THE GEDIZ GRABEN, WESTERN ANATOLIA, TURKEY

A Thesis Submitted to the

Graduate School of Natural and Applied Sciences of Dokuz Eylül University In Partial Fulfillment of the Requirements for the Degree of Master of Science in Geological Engineering, Applied Geology Program

by

Hüseyin UYTUN

October, 2021

İZMİR

M.Sc THESIS EXAMINATION RESULT FORM

We have read the thesis entitled **"RELATION BETWEEN INDUCED SEISMICITY AND GEOTHERMAL SYSTEMS: A CASE STUDY FROM THE GEDIZ GRABEN, WESTERN ANATOLIA, TURKEY"** completed by **Hüseyin UYTUN** under supervision of **PROF.DR. HASAN SÖZBİLİR** and **PROF.DR. ALPER BABA** and we certify that in our opinion it is fully adequate, in scope and in quality, as a thesis for the degree of Master of Science.

Prof. Dr. Hasan SÖZBİLİR	Prof. Dr. Alper BABA
Supervisor	Co-Supervisor
Prof. Dr. Orhan TATAR	Prof. Dr. Talip GÜNGÖR
Jury Member	Jury Member

Dr. Öğretim Üyesi Murat TOKÇAER

Jury Member

Prof. Dr. Özgür ÖZÇELİK

Director

Graduate School of Natural and Applied Sciences

ACKNOWLEDGEMENTS

First of all, I would like to express my grateful thanks to my supervisors Prof. Dr. Hasan SÖZBİLİR and Prof. Dr. Alper BABA for not only their valuable suggestions and assistance during the research, but also for they support and encouraging me. Their recommendations helped me in all the time of research and writing of this thesis. They were patient and invested much time and let me to consult they any time during my studies even when they were busy.

I also would like to thank the colleagues for their support and help throughout the study. Additionally, I would like to thank sincerely to my best-friends for their friendship and motivation in every part of the study. Finally, I would like to declare my appreciation to my family for their patience, support and help during my life.

This thesis would never have been completed without these people's supports, thanks to everyone individually.

Hüseyin UYTUN

RELATION BETWEEN INDUCED SEISMICITY AND GEOTHERMAL SYSTEMS: A CASE STUDY FROM THE GEDIZ GRABEN, WESTERN ANATOLIA, TURKEY

ABSTRACT

It is well known that pore pressure and stress variation trigger earthquakes when a potentially active fault or crack is in critical equilibrium. This study examines the effects of geothermal energy activities on seismicity, which accelerated in the Gediz Graben in 2011-2012. Geothermal fluid in Gediz Graben comes into existence from tectonic zones of low angle Gediz Detachment Fault (GDF) of Quaternary age and high angle normal faults of Holocene age. For indirect and direct use of geothermal energy, many wells with production and reinjection functions have been drilled in the Gediz Graben (GG) at depths of 600-4300 m. Geothermal production, reinjection, and seismic data were assessed together with the structural geology of the study area by using the Geographic Information System-based programs. These results show that an increase in seismicity was observed simultaneously with the excavation and testing of geothermal wells.

It was terminated that earthquakes of 0.9 - 3.4 magnitude in the study area may be related to geothermal activity. In addition to the geothermal production - reinjection process, micro-earthquakes were observed during the drilling operations and well tests, which may occur due to the reactivation of pre-existing faults.

Regarding the geothermal power plants in Gediz Graben, the relationship between geothermal production, reinjection activities, and seismicity should be determined, predicted, and controlled by the "traffic light" system.

Keywords: Induced seismicity, active fault, geothermal, reinjection.

TETİKLENMİŞ DEPREMSELLİK VE JEOTERMAL SİSTEMLER ARASINDAKİ İLİŞKİ: GEDİZ GRABENİ ÖRNEĞİ, BATI ANADOLU, TÜRKİYE

ÖZ

Potansiyel olarak aktif bir fay veya çatlak kritik dengede olduğunda boşluk basıncı ve gerilme değişiminin depremleri tetiklediği iyi bilinmektedir. Bu çalışma, 2011-2012 yıllarında Gediz Grabeni'nde hızlanan jeotermal enerji faaliyetlerinin sismisite üzerindeki etkilerini incelemektedir. Gediz Grabeni'ndeki jeotermal akışkan, Kuvaterner yaşlı düşük açılı Gediz Ayrılma Fayı'nın (GDF) tektonik zonlarından ve Holosen yaşlı yüksek açılı normal faylardan meydana gelmektedir. Jeotermal enerjinin dolaylı ve doğrudan kullanımı için 600-4300 m derinliklerde Gediz Grabeninde (GG) üretim ve reenjeksiyon fonksiyonlu çok sayıda kuyu açılmıştır. Jeotermal üretim, reenjeksiyon ve sismik veriler, Coğrafi Bilgi Sistemi tabanlı programlar kullanılarak çalışma alanının yapısal jeolojisi ile birlikte değerlendirilmiştir. Bu sonuçlar, jeotermal kuyuların kazılması ve test edilmesiyle eş zamanlı olarak sismisitede bir artış gözlemlendiğini göstermektedir.

Çalışma alanındaki 0,9 - 3,4 büyüklüğündeki depremlerin jeotermal aktivite ile ilişkili olabileceği sonucuna varılmıştır. Jeotermal üretim - reenjeksiyon işlemine ek olarak, sondaj çalışmaları ve kuyu testleri sırasında, önceden var olan fayların yeniden aktif hale gelmesi nedeniyle oluşabilecek mikro depremler gözlemlenmiştir.

Gediz Graben'deki jeotermal santrallerle ilgili olarak, jeotermal üretim, reenjeksiyon faaliyetleri ve sismisite arasındaki ilişki “trafik ışığı” sistemi ile belirlenmeli, tahmin edilmeli ve kontrol edilmelidir.

Anahtar kelimeler: Tetiklenmiş depremsellik, aktif fay, jeotermal, reenjeksiyon.

CONTENTS

Page

LIST OF FIGURES

Page

LIST OF TABLES

Page

CHAPTER ONE

INTRODUCTION

1.1 Purpose and Scope

Geothermal energy is a proven thermal energy resource for direct use and power generation which is generated and stored on earth. The earth's heat originates from radioactive decay and heat flow from geological units (Davies & Rhodri, 2010). Mankind utilizes geothermal energy for thousands of years (Baba, 2015). According to archaeologists, the first human use of geothermal resources worldwide occurred thousands of years ago. Geothermal utilization developed in different places as cooking, washing, bathing, and similar uses throughout history (Baba & Armannsson, 2005). In the early twentieth century, geothermal power generation was started in Larderello, Italy. In recent years geothermal utilization has reached enormous sizes. It has also been revealed that the use of geothermal activities causes seismicity, especially with the increase and widespread use of energy production.

The type of seismicity caused by human activities or that triggers faults in critical conditions is induced or induced seismicity. Many different human activities can cause triggered seismicity. The reservoir behind dams, wastewater injections, oil/gas operations such as hydraulic fracking and mining, and geothermal generation-injection activities can cause earthquakes (Zoback, 2007).

Seismicity induced by geothermal generation or injection is known to occur when the fluid pressure in a fault or crack reaches a critical value where it exceeds the friction that prevents fault slipping.

Doglioni (2018) states that at least four different types of human activity can be identified that can cause seismicity:

> (1) fluid removal from a stratigraphic reservoir in the underground can trigger the compaction of the voids and the collapse of the overlying volume i.e., graviquakes; the deeper the reservoir the bigger the volume and the earthquake magnitude; (2) wastewater or gas reinjection provides the reduction of friction in volumes and along fault planes, allowing creep or sudden

> activation of tectonic discontinuities, i.e., reinjection quakes; (3) fluid injection at supra-lithostatic pressure generates hydrofracturing and micro-seismicity, i.e., hydrofracturing quakes; (4) fluid extraction or fluid injection, filling or discharging of artificial lakes modifies the lithostatic load, which is the maximum principal stress in extensional tectonic settings, the minimum principal stress in contractional tectonic settings, and the intermediate principal stress in strike-slip settings, i.e., loadquakes; over given pressure values, the increase of the lithostatic load may favour the activation of normal faults, whereas its decrease may favour thrust faults (Doglioni, 2018).

"Triggered" and "induced" seismicity is distinguished by some researchers based on whether some or all of the energy generated by the earthquake is anthropogenic. It is clear that the source of energy emitted or released during major earthquakes is tectonic, but it is difficult to replace how much of the energy is natural and how much is anthropogenic. The term "induced" is used for both cases, which is in keeping with the convention of the Committee on Induced Seismicity Potential (Hitzman, 2013). In this study, all anthropogenic seismicity is considered as induced seismicity. Figure 1.1 shows the relation to human activities seismicity. The result indicates that especially dam and extraction fluid in-ground triggered the earthquake.

The number of triggered earthquake events observed to date and reported to the literature is about 1000 worldwide. As the above chart indicates that large earthquakes can occur with human intervention. The most significant triggered earthquakes are caused by dams. Fracking was recently recorded as the most triggered seismicity-producing activity (IEO, 2020). The use of geothermal energy is one of the important factors causing triggered seismicity (Doglioni, 2018). According to Bromley (2012), considering active tectonic environments, high levels of natural seismicity are common, faults can be pre-stressed, and seismicity can be triggered by induced stress changes. The magnitude and number of seismicity depend on natural factors such as local stress, friction, fault orientations, and locations. Factors affecting seismicity are displacement stresses from volumetric contraction caused by fluid extraction (HM Coupling); thermal stress created by injection of cool fluids into hot rock (TM Coupling); and chemical stresses associated with injection of brines or acid fluids (CM Coupling, see Figure 1.2), causing mechanical degradation of rock or stress relief. On the other hand, there are controllable factors such as injection pressure-temperature and volume of injected fluid (Bromley & Majer, 2012).

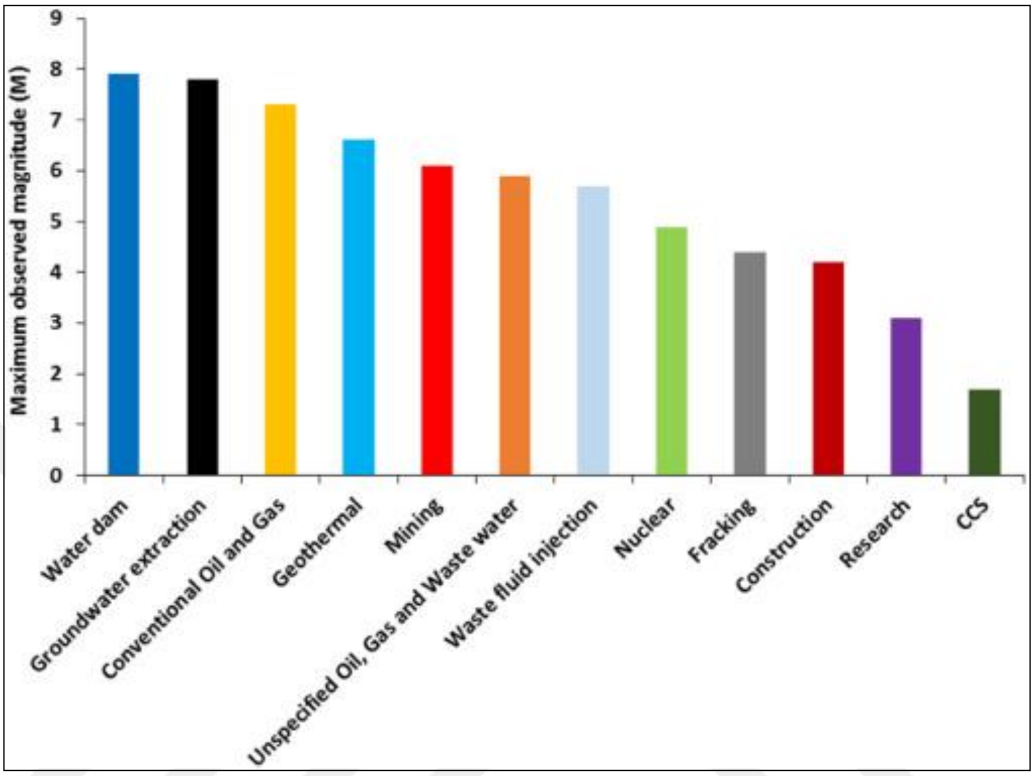

Figure 1.1 The maximum observed induced seismicity magnitudes and human activities (CCS : Carbon capture and storage) (IEO, 2020)

McClure & Horne (2012) point out that "induced seismicity occurs when stress is changed on pre-existing fractures so that their shear traction exceeds their frictional resistance to slip according to the Coulomb failure criterion":

$$\tau = \mu(\sigma_n - P) + S \qquad 1.1$$

Where τ is shear traction on a fracture [Pa], σ_n is normal stress [Pa], P is fluid pressure [Pa], S is the fracture cohesion, and m is the coefficient of the friction [-]. When the failure criterion is exceeded on a fracture, slip occurs to relieve shear stress (McClure & Horne, 2012; Jaeger *et al.* 2007)". According to the equation 1.1, seismicity is triggered by shear stress, normal stress, or fluid pressure change.

Triggered seismicity is directly related to the properties of the rock matrix, the properties of the fracture-crack system, temperature, and stress changes. Kaiser effect phenomenon is that when rock cores are loaded in uniaxial compression, acoustic emission occurs when the stress reaches a level greater than that which the rock has previously experienced (Lehtonen & Cosgrove, 2012). According to Zang *et al.* (2014) "stress magnitudes are essential in multiple stimulations of wells where little or no seismicity is observed until the previous maximum stress level is exceeded (Kaiser Effect).

Hydraulic fracturing or fracturing operations have been applied to enhance the permeability of reservoir rocks by injection of water with high pressures. Due to that injection, new cracks and fractures in the reservoir can be generated via altering effective stress distribution, triggering seismicity with magnitudes approximately 2 - 3. According to Matsugana *et al.* (1993), hydraulic fracturing is the most common method used to create an artificial fracture for extracting heat from a Hot Dry Rock (HDR) geothermal reservoir.

Hydromechanical interaction processes in the reservoir are shown in Figure 1.2. Although the process always moves in both directions, a particular direction may be dominant depending on the particular situation.

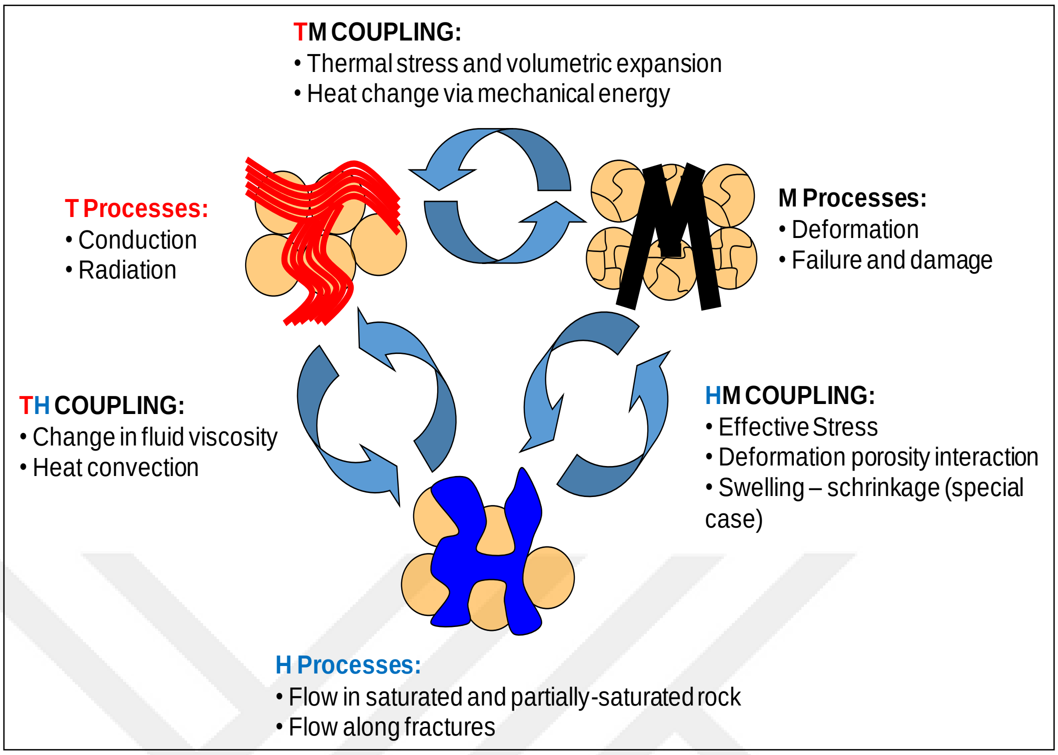

Figure 1.2 General illustration of Thermo-Hydro-Mechanical (THM) coupling processes in a rock excluding chemical coupling (Konietzky & Yildizdag, 2018)

Turkey is located in one of the most seismically active regions globally, has a considerably high level of geothermal energy potential thanks to its geological and tectonic settings. Turkey is located within the Mediterranean Earthquake Belt, the complex deformation resulting from the continental collision between the African and Eurasian plates (Bozkurt, 2001; Baba & Sözbilir, 2012). The border of these plates constitutes seismic belts marked by young volcanic and active faults, allowing the circulation of water and heat. The distribution of hot springs in Turkey roughly coincides with the distribution of the fault systems, young volcanism, and hydrothermally altered areas (Simsek, 2009; Baba, 2015). The relationship of geothermal resources with earthquakes has attracted attention in recent years, and studies on these issues are increasing. This study focuses on the relationship between geothermal activity and seismicity in the activity tectonic zones of the Gediz Graben (GG) located in Western Turkey.

As it is widely accepted, geothermal energy is a sustainable, clean, and cheap energy source and can be used directly or indirectly. Therefore, it has developed rapidly in Turkey as well as research and the use of geothermal energy in the world. The case study is conducted in the Gediz Graben in the western part of Turkey; despite having rich geothermal resources due to the geological characteristics, its geothermal resource utilization has been restricted to balneology, greenhouses, and districted heating systems until geothermal "Law on Geothermal Resources and Natural Mineral Waters" and its Implementation Regulations released. The study aims to compare and interpret seismic data and geothermal data and investigate the relationship between seismicity and geothermal energy use in GG.

1.2 Geographical Setting of the Study Area

The study area is located in the GG, the western part of Turkey (Figure 1.3). The Gediz Graben is a 150 km long, 3–40 km wide, approximately E–W trending structure and forms one of the most prominent structural elements of western Turkey.

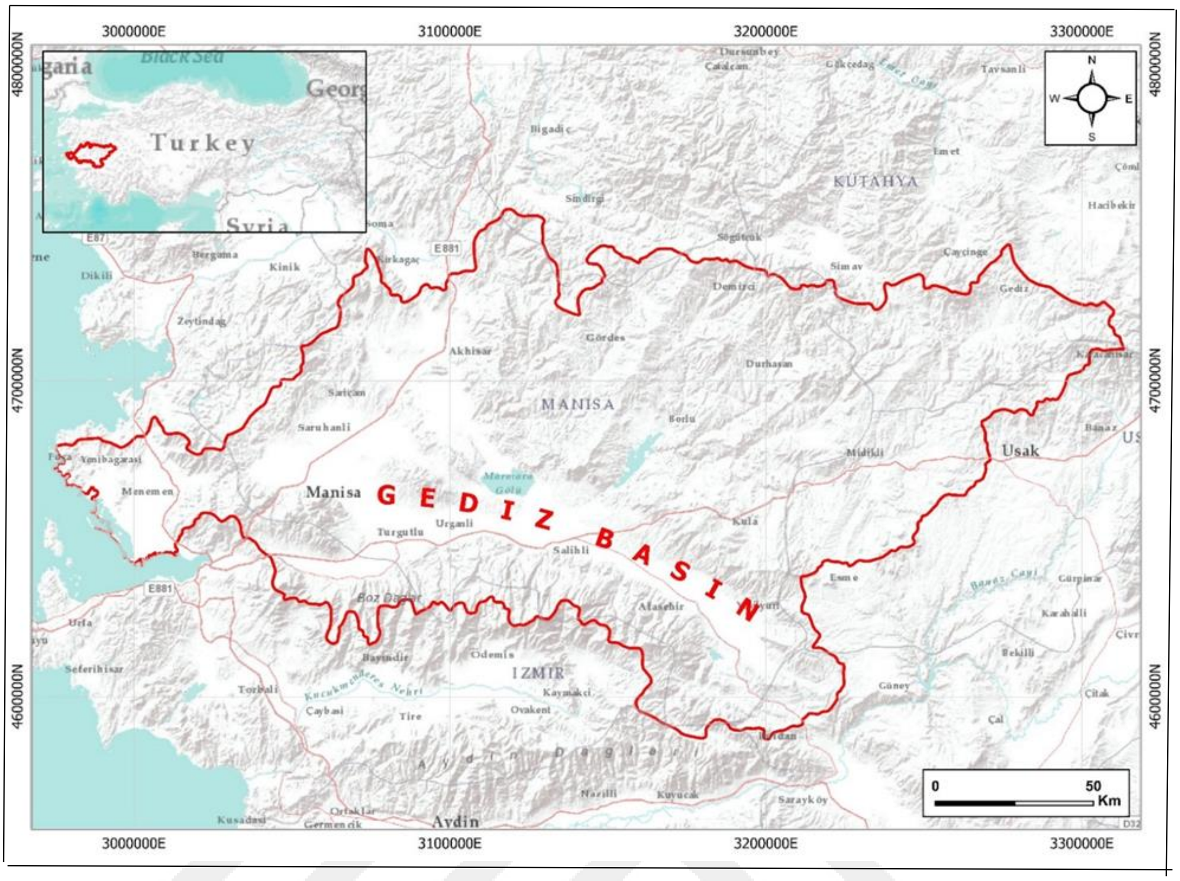

Figure 1.3 Location map of the study area

1.3 Previous Studies

Many scientists worked in this region. Most of the study was done about geology and tectonics (Arpat & Bingol, 1969;   Mc Kenzie, 1978; Şengör & Yılmaz, 1981; Emre, 1996; Emre & Sözbilir, 1997; Yılmaz, 2000; Sözbilir, 2001; Seyitoglu et al., 2000; Bozkurt & Sözbilir, 2004; Çiftçi & Bozkurt, 2009; Seyitoğlu & Işık, 2015). Also, several studies were carried out about the hydrological, hydrogeochemical, and geochemical features of geothermal fields in the Graben (Karamanderesi & Yılmazer 1983; İztan & Yazman, 1990; Tarcan et al. (2000); Özen et al. (2012); Baba (2015); Eser Project Report (2014); Orakcı et al. (2019); Rabet et al., (2017).

Arpat & Bingöl (1969) examined the 1969 earthquake in the study area and suggested that the Alaşehir valley was a graben.

McKenzie's study (1978) shows that E-W, NW-SE, NE-SW extending normal faults are effective in the formation of the current morphology of Western Anatolia, which is an expansion region.

Şengör & Yılmaz (1981) revealed the relationship between the N-S extension in the Aegean region and the westward escape of the Anatolian Plate bounded by the North Anatolian Fault and the Eastern Anatolia Fault.

In the study of İztan & Yazman (1990), the basin pattern was revealed by using seismic studies for petroleum purposes in the basin. According to this, pre-Miocene bedrock consists of Menderes Massif metamorphic rocks and ophiolitic rocks of İzmir-Ankara Zone in the basin.

According to Emre (1996) Gediz Graben is an NW - SE. It is a half-graben, and the youngest sediments of the graben from the Alaşehir Plain and the extension of the Gediz Graben begins with the formation of the Karadut Fault, the youngest detachment fault in the region.

The argument that the large-scale, low-angle Gediz detachment fault forming the southern edge of the Gediz graben has elongation-based macroscopic structures such as folds and backward-inclined layers were put forward by Sözbilir (2001). It has been reported that the folds are formed as antiformal and isomorphic structures with both parallel and vertical axes to the direction of extension in the base walls and suspended walls, respectively.

In the field studies carried out in the south of Alaşehir by Bozkurt & Sözbilir (2004), kinematic data revealed that the Alaşehir formation covers the rocks of the Menderes Massif with a low angle normal fault.

According to Çiftçi & Bozkurt (2009), there are three different Neogene sub-basins divided from one another by transfer faults under alluvium in the vicinity of Alaşehir, Salihli, and Turgutlu.

CHAPTER TWO
GEOLOGY OF THE STUDY AREA

2.1 Geological Setting

Turkey lies in a significant region on the western segment of the Alpine-Himalayan Orogenic Belt. Hellenides and Carpathians branches of the Alpine system cross Turkey in complex Tauride and Pontide blocks and connect with the Bitlis-Zagros zone to the east. Compressional, strike-slip, and local extensional deformations are observable throughout the entire Alpine-Himalayan Orogenic Belt driven by the complicated convergence of Africa and Eurasia (Şengör & Yılmaz, 1981).

The Aegean Region has been suffering from the active N-S extensional tectonics, under the control of two main motions. One of them is the westward escape of the Anatolian Plate, bounded by the North Anatolian Fault and the East Anatolian fault, intersecting at the Karlıova depression of East Anatolia. The rate of this motion is about 20-25 mm/year (Şengör & Yılmaz, 1981). The westward motion changes the direction in West Anatolia with a rather abrupt anticlockwise rotation, toward southwest over the Hellenic Trench. The other motion is the North-South extension of the Western Anatolia and the Aegean with a rate of about 3-6 cm/year (Yılmaz, 2000).

As a consequence of these motions, a group of approximately east-west trending grabens has been developing (Yılmaz, 2000). Gediz Graben is one of the best-developed grabens in Western Turkey. Almost the entire section of the graben fill is exposed along its southern margin, revealing many aspects of the depositional system and the extensional deformation (Çiftçi & Bozkurt, 2009).

According to Uzel et al. (2013), The Izmir-Balıkesir Transfer Zone is a conjugate strike-slip fault that transmits the deformation difference between the Cycladic and Menderes Metamorphic core complexes. Uzel et al. To better define the role of İBTZ in the region. Miocene volcano-sedimentary rocks and granitic using new paleomagnetism data collected from rocks analyzed the history of rotation. The analysis results have been carried out from the Miocene to the present reveals that there is a rotation phase (Özkaymak & Kaymakçı, 2013). As Seyitoğlu & Işık (2015) has noted, the Aegean region (including Western Anatolia, Aegean Sea, and Greece) is one of the areas of the earth under the effect of extensional tectonics and the extensional area includes the typical features of core complexes in this type of region. The Menderes Massif in Western Anatolia was exhumed initially as an asymmetric core complex in the Early Miocene due to extension beginning in the Oligocene, and then the central Menderes Massif was further exhumed as asymmetric core complex.

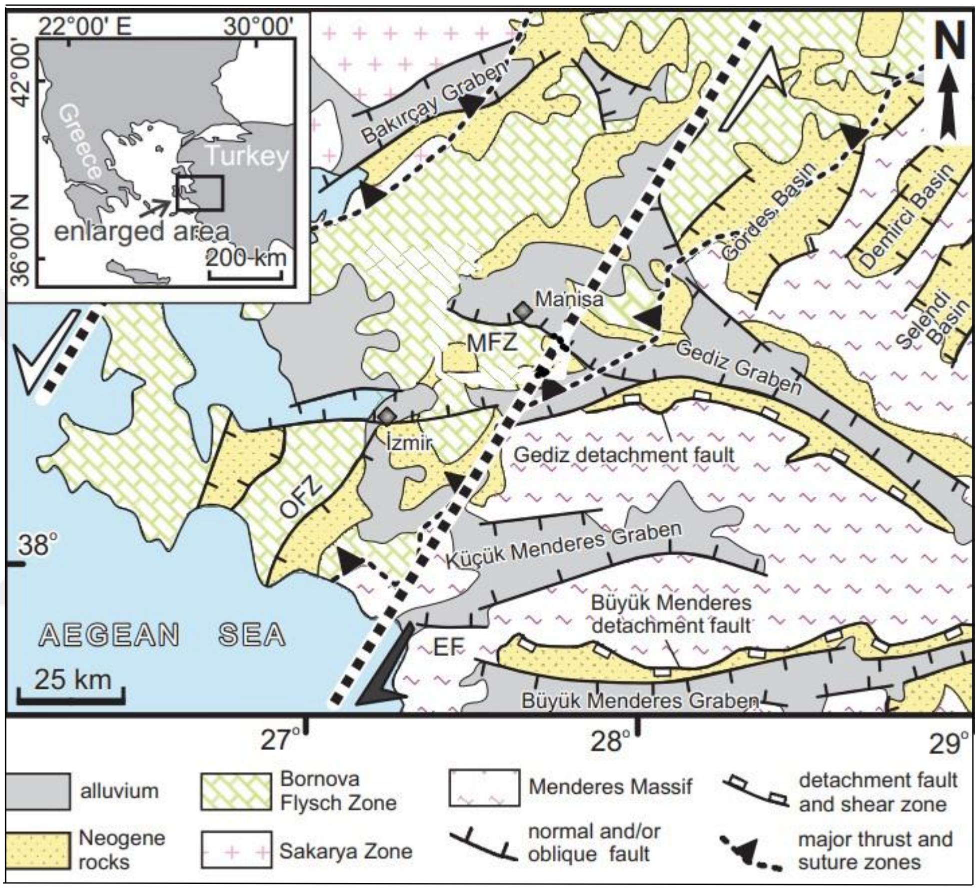

Figure 2.1 Geological map of western Turkey showing major tectonostratigraphic units and surroundings of the study area (Özkaymak & Sözbilir, 2008)

2.2 Geology of the Gediz Graben

Gediz Graben is located in Manisa, which belongs to West Anatolia (see Figure 2.1). At the regional scale, the Gediz Graben comprises the main depression of the surface drainage system of the Gediz Basin. The Alaşehir section of the Gediz Graben, which possesses the largest alluvial area in the Gediz Basin, is 140 km long and 5 to

15 km wide. The graben extends in the NW-SE direction between Sarigol and Alasehir in the west, and it is divided into two main branches from the town of Salihli towards the west. The Southernmost branch extending in the E-W direction is divided into two branches, namely the Kemalpasa Basin and the Manisa Basin as from the Town of Turgutlu. The branch extending in the NW-SE direction from the Town of Salihli is known as the Golmarmara Basin. The Miocene period units of these sub-basins include the same Quaternary Alluvial unit, and the basin fill sequences offer differences in the horizontal and vertical directions. According to the Turkish Petroleum Corporation's deep seismic cross-sections (Çiftçi & Bozkurt, 2009), it has been found out that there are three different Neogene sub-basins divided from one another by transfer faults under alluvium in the vicinity of Alasehir, Salihli, and Turgutlu. The seismic data showed that the easternmost basin starts in the east of Sarigol and extends as far as Derekoy towards the northwest. The basin deepening again towards Salihli pasts a transfer fault extending in the NE-SW direction closes around Sardis. Here, the Turgutlu-Ahmetli sub-basin starts through a second transfer zone. According to these data, three depressions are remaining from the Neogene period under the Alasehir (Gediz) Graben, which is observed as a single alluvial basin along the Sarigol-Alasehir-Salihli-Turgutlu line (Sözbilir, 2015 unpublished report). A significant number of studies have been carried out on the stratigraphy of the section of the Gediz Graben between Alasehir and Sarigol. In such studies, the formations belonging to these made by Yazman et al. (1990) have reached the present day with a little change. The sequence set according to this study has been combined with the seismic surveys carried out for petroleum extraction purposes in the basin and the basin pattern has been thus revealed. Accordingly, the pre-Miocene base rocks are comprised of the metamorphic rocks of the Menderes Massif and the ophiolitic rocks of the Izmir-Ankara Zone in the basin. The Miocene-Quaternary sedimentary fill of the basin is the Alasehir formation, Çaltılık formation, Gediz formation, Kaletepe formation, Bintepeler formation, and alluviums from the bottom to the top (Figure 2.2). The oldest sedimentary unit is the Alaşehir Formation, which is cropping out on the southern margin of the Gediz Graben.

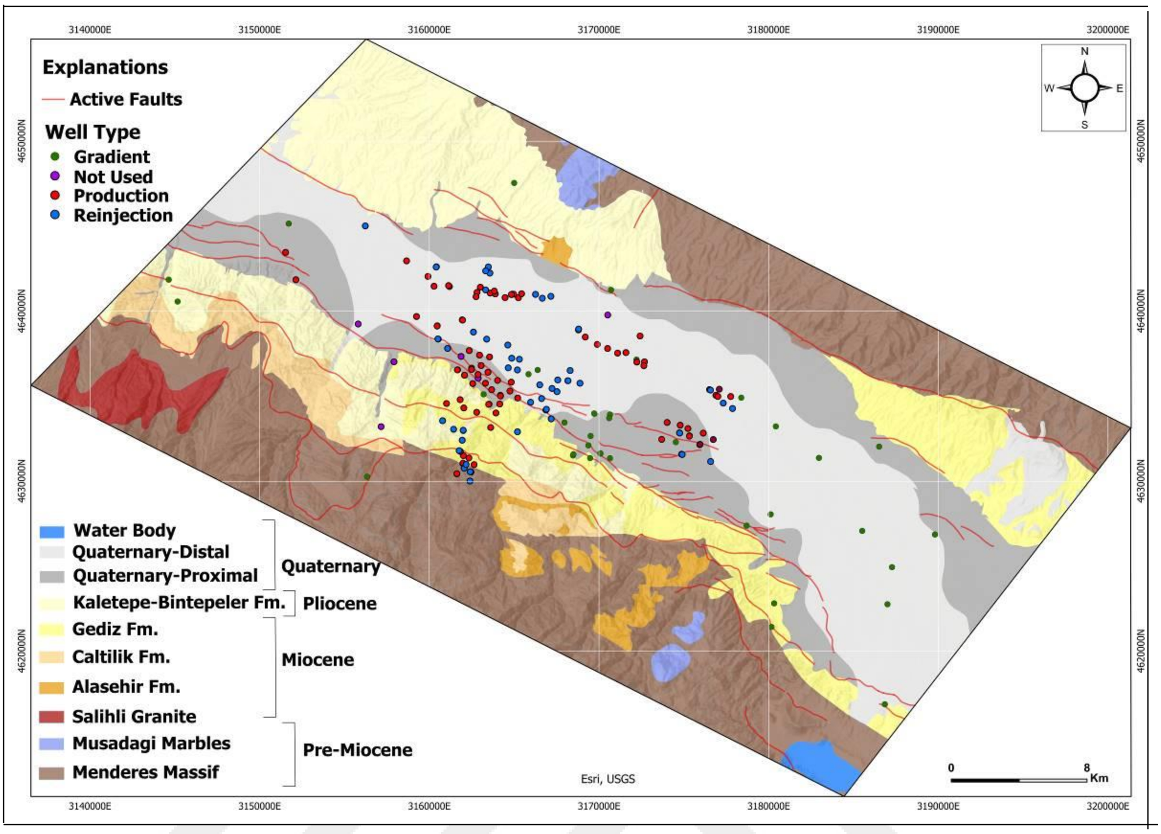

Figure 2.2 Geological map of the study area (modified from Eser Project, 2014)

2.3 Stratigraphy of the Gediz Graben

The Gediz graben has a WNW–ESE trending structure bounded by active normal faults. The Gediz detachment, which is located along a discontinuous trace along the fault for more than 100 km from Turgutlu to Alaşehir district, is one of several crustal-scale detachment faults that were formed at the edge of the southern basin of the Gediz graben (Koçyiğit et al., 1999; Sözbilir 2001). The Gediz detachment's footwall comprises mylonitic gneiss, marble, and schist of the Menderes metamorphic core complex and Miocene synextensional granite. The hanging wall of the detachment fault comprises Miocene to Quaternary sedimentary units are reaching up to 2500 m thick (Baba & Sözbilir, 2012). When examined based on previous studies in the study area, the outcropping rocks can be grouped into two main groups: basement rocks and sedimentary cover rocks (Figure 2.3 & Figure 2.4). The bedrock in the study area is aged before Miocene, while sedimentary cover rocks are Miocene and Pliocene age.

The basement rocks consist of Precambrian-lower paleozoic aged Augen gneiss, migmatite gneiss, granite, granitic gneiss, mylonitic gneiss belonging to the Menderes Massif. Above this are rocks composed of Upper Paleozoic-Middle Triassic micaceous-schist, quartzite, quartz-schist, and marbles. Neogene aged sedimentary rocks emplaced with angular unconformity on top of the Menderes Massif. The unit at the top of the stratigraphic sequence in the study area is alluvium and travertine.

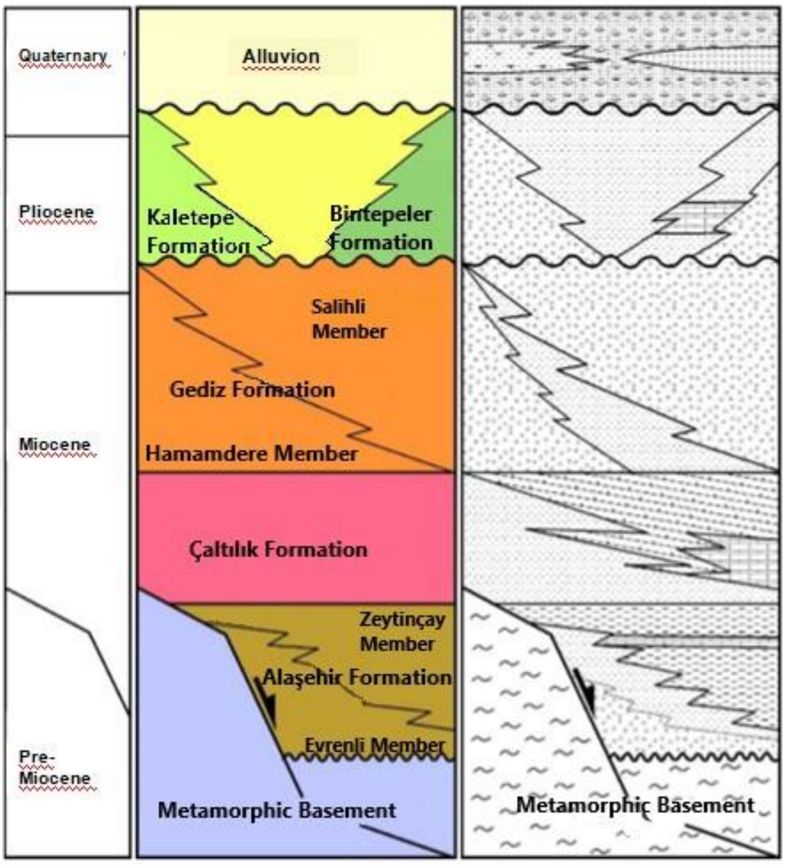

Figure 2.3 Stratigraphic Column of Study Area (Çiftçi and Bozkurt, 2009)

2.3.1 Menderes Massif

The Menderes massif, which spreads to the S-SE and north of the study area and is the oldest unit in the Gediz Graben, consists of gneiss, schist, calc-schist, quartz-schist, and marbles. The age of the Menderes Massif is accepted as Paleozoic-Mesozoic, according to Yazman & Iztan (1990). Schists and calcschists defined as cover schists of the Menderes massif show a wide distribution in the study area. The sample taken from the central parts of the mica-schist unit was defined as sericite-chlorite-muscovite-quartz schist (Karamanderesi et al., 1995). The unit, which can be seen as gray, greenish-gray, brown, light brown, consists of garnet schist, quartz schist, calcschist, crystallized limestone, and marble bands. Schists, calcschists, and marbles, which present lateral and vertical facies changes, are of upper Paleozoic age according to the stratigraphic relationship. Salihli Granit and Musadağı Marbles are members of the Menderes massive, which contain geothermal brine and cropped out SW of the Gediz Graben.

2.3.2 Alaşehir Formation

The Alaşehir formation, defined by Yazman & İztan (1990), is the oldest Neogene unit in the study area, and it generally outcrops in the southeast of the graben. The Alaşehir Formation of the early-middle Miocene age starts with conglomerate at the bottom and continues with sandstone, siltstone, shale, and marl. The contact between the metamorphic rocks forming the Menderes Massif and the Alaşehir formation has been defined as the unconformity with faults (Iztan & Yazman, 1990; Yilmaz et al., 2000; Seyitoglu et al., 2002). Seyitoglu et al. (2002) proved for the first time that this contact between the Alaşehir formation and the basement rocks is a low-angle normal fault. Later, Bozkurt & Sözbilir (2004) revealed that the Alaşehir formation covered the rocks of the Menderes Massif with a low angle normal fault with kinematic data in the field studies conducted in the south of Alaşehir. In later studies (Çiftçi, 2009), it is accepted that the Alaşehir Formation structurally covered the Gediz Detachment Fault. In recent field studies in the region (Çiftçi, 2009), the coarse-grained facies of the Alaşehir formation have been identified as the Evrenli member and the fine-grained facies as the Zeytincay member.

2.3.3 Çaltılık Formation

The Çaltılık Formation overlies the Alaşehir Formation with a transitional contact characterized by sandstones and pebble stones with limestone lenses. The Çaltılık

Formation was first identified at the Çaltılık Village by Yilmaz et al. (2000). According to Seyitoğlu et al. (2002), the Kurşunlu formation contains both the Çaltılık and the Gediz formations. Caltilik Formation and Alasehir Formation, the age has been found to be 15.5 My (Seyitoğlu et al. 2002).

2.3.4 Gediz Formation

The Gediz Formation extends along the southern margin of the graben along a line limited by NW-SE oriented and north-trending normal faults. The Gediz Formation was first identified as the Gediz group by Iztan & Yazman (1990). According to the authors, the Gediz group is comprised of the Hamamdere and Salihli formations. These two formations consist of a conglomeratic alluvial fan system and sandy fluvial system, respectively. Yilmaz et al. (2000) use the designation of the Kızıldağ group for this lithology. On the other hand, Koçyiğit et al. (1999) studied the same group under the designation of Saglikdere, Kartaluçan, Acıdere and Göbekli formations. According to Seyitoğlu et al. (2002), the Kurşunlu formation contains both the Çaltılık and the Gediz formations.

2.3.5 Kaletepe Formation

The Kaletepe Formation extends in the form of a strip along the southern margin of the Gediz graben. The Kaletepe Formation was first identified by Iztan & Yazman (1990), and then the same formation was studied under the designation of the Sart group in Yilmaz et al. (2000), Sart Formation in Seyitoglu et al. (2002), and Asartepe Formation in Emre (1996) and Koçyiğit et al. (2000). The Kaletepe Formation is characterized by a less-consolidated conglomerate with multi-exemplary components and interlayers of sandstone and mudstone at small percentages. The unit overlies the Gediz Formation with angular unconformity.

2.3.6 Bintepeler Formasyonu

The Bintepeler Formation crops out on the northern margin of the Gediz graben. The formation was first mapped and designated by İztan & Yazman (1990). The Bintepeler formation unconformably overlies the rocks of the Menderes Massif starts with a coarse-grained conglomerate on the basement, and limestone prevails with the finning grain size towards the top.

2.3.7 Quaternary Alluvium

The alluviums comprising the current fill of the Gediz Graben may be studied under two main facies a lateral alluvial fan and axial fluvial sediments. Lateral alluvial fans are observed along the southern and northern margins of the Gediz Graben. The fans are made up of clastic materials deriving from the host rising along the margin of the graben. These sediments have developed under the control of the Alasehir River to penetrate the axial fluvial sediments in horizontal and vertical directions towards the center of the graben. Alluvial fans combined in various sizes are defined as Proximal Quaternary alluvium. Distal Quaternary alluvial channel filling sands and young sediments are consisting of fine-grained flood sediments. Quaternary travertines also crop out in the south and north of the study area, especially near faults.

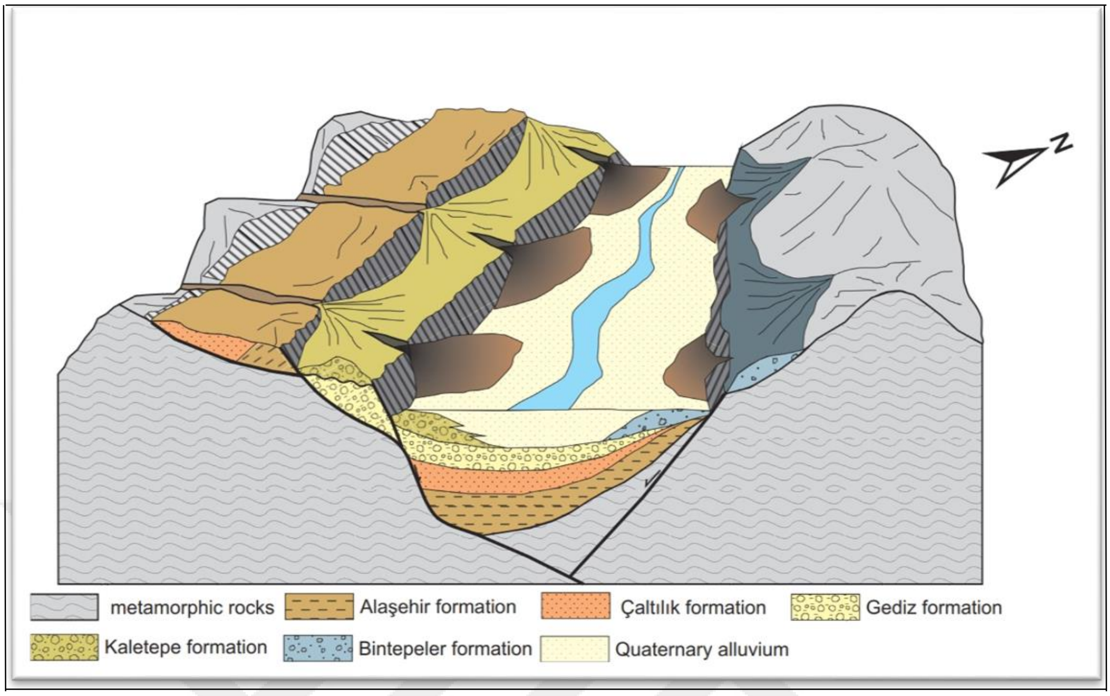

Figure 2.4 Schematic block diagram of the Gediz Graben (Çiftiçi & Bozkurt, 2009)

CHAPTER THREE

HYDROGEOLOGY OF THE STUDY AREA

3.1 Surface Water Resources

The study area located in the southeast part of the Gediz basin is of Mediterranean climate type in terms of microclimate. Summers are hot and dry, winters are warm and rainy, except for the higher parts of the basin. Rainfall is generally seen as rain, rarely as short-term snow. The plants in the region vary depending on the height; These are lowland plants, maquis, drought-resistant, and permanently green Mediterranean plants and forests.

Within the scope of this study, the rivers that constitute the main drainage network of the Alaşehir part of the Gediz Basin have been accepted as the main water points. In addition to these, the dam lakes in the basin are examined as essential water points in the basin. The water usage in the basin is mostly provided by groundwater.

3.1.1 Rivers

The mainstream in the study area is Alaşehir Stream. Rivers such as Alkan Stream, Şahyar Stream, Zeytin Stream, and Kurudere Stream join with Alaşehir Stream in the central part of the basin. The Gediz Stream merges with the Alaşehir stream, draining the southeast of the basin near Salihli and is named Gediz River.

3.1.2 Dams and Ponds

Many water structures of different purposes and sizes have been built in the basin. The most important of these structures are the dams built for energy production, agricultural irrigation, and drinking water. Apart from dams, ponds built for agricultural irrigation and flood protection and mooring structures (regulators) built for transferring water to agricultural irrigation facilities are also among the important water structures of the basin. Among the dams and ponds near the study area, the most important dam is the Demirköprü Dam, the largest water structure in the basin. Afşar Dam is the second important water structure in the southeast of the basin. It is a zoned landfill type dam built for irrigation and flood protection.

3.2 Groundwater Resources

Geothermal systems and freshwater aquifer systems interact together in the study area. Alluvial Aquifers, which have primary porosity in terms of freshwater, have an important place in the study area. It has been observed that hot springs in the study area are generally associated with young faults and metamorphic rocks. The geothermal reservoir in the region mainly consists of fractured marble levels. Besides, gneiss, schist, quartzite may contain geothermal fluid, depending on the secondary porosity that develops due to the fracture-crack system. Although the main reservoir is in the bedrock, they can form geothermal reservoirs due to the development of fracture-crack systems in the limestone and conglomerate levels of the Alaşehir Formation. In terms of geothermal systems, the impermeable clayey levels of the basin-fill sediments form the cover rock. Since the Alaşehir Formation does not contain a fracture-crack system, the parts that do not develop secondary porosity are impermeable. The basement rocks that outcrop in the north and south of the study area and the cover units with no fracture-crack system form impermeable units in terms of freshwater aquifer systems (Figure 3.1).

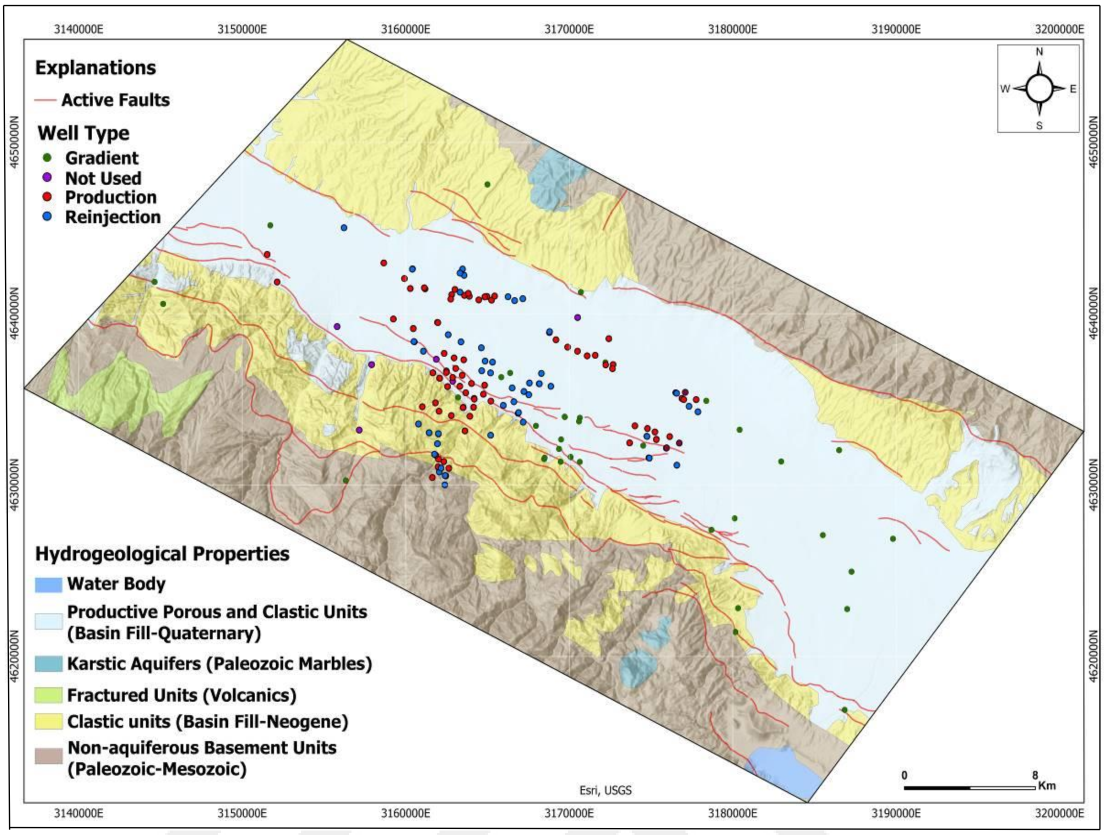

Figure 3.1 Hydrogeological map of the study area (modified from Eser Project, 2014)

3.2.1 Non-aquiferous Basement Units (Paleozoic-Mesozoic)

The mica schists, quartz schists, and gneisses that do not show fractured features intercalated with the marbles in the Menderes Massif have low porosity and permeability. On the other hand, Paleozoic-Mesozoic basement units, which have developed fracture-crack systems due to tectonic effects in places close to fault zones, may show the feature of the reservoir.

3.2.2 Clastic Units (Basin Fill - Neogene)

The clastic units located in the south of the study area have a fractured-fractured structure along the detachment fault zone and are reservoirs. The permeability and porosity properties of the clastic units are determined according to the binding material and the amount of the clay-sized material.

3.2.3 Fractured Units (Granite – Granitic Gneiss)

Rocks such as granite, granitic-gneiss, which are exposed in the south of the study area, have acquired secondary porosity and permeability in places close to faults and show reservoir characteristics.

3.2.4 Karstic Aquifers (Paleozoic Marbles)

In addition to their karstic features, Paleozoic Marbles form the main reservoir in the geothermal system in the study area with the development of the fracture-crack system close to the fault zones. They are located in the Menderes Massif, and in some cases, they can be intercalated with mica-schist and quartz-schist.

3.2.5 Productive Porous and Clastic Units (Basin Fill-Quaternary)

The Neogene basin fill and the loosely attached sandy-gravelly parts of the Quaternary units have porosity and permeability and show reservoir characteristics. Low porosity parts of these units, such as thin claystone and siltstone, are impermeable and serve as cover rocks.

3.3 Hydrogeochemistry

Hydrogeochemical studies of groundwater and surface waters were carried out in the Hydrogeological Assessment of the Gediz Watershed Project in 2014 (Eser, 2014), based on the entire Gediz basin. The findings obtained in this context are briefly summarized in this section. In the Geothermal Fluid section, permission was obtained by Manisa YIKOB to be used in the study, and a summary was prepared by compiling geothermal well and resource data.

3.3.1 Surface Water

Generally, it is seen that surface waters are rich in Ca-HCO_3 ions. It provided similar data on the origins of the surface waters obtained from both the Piper and Schoeller diagrams (Figure 3.2 and Figure 3.3). Calcium, magnesium, sodium and potassium values were ranged from 8,08–458.29 mg/L; 0.5–159.91 mg/L; 1.13–406.21 mg/L to 0.09–57.91 mg/L, respectively. Bicarbonate, sulphate, and chloride concentrations in surface waters were range between 25.23–1103.49 mg/L; 2.55–1450 mg/L and 0.88 - 513 mg/L, respectively.

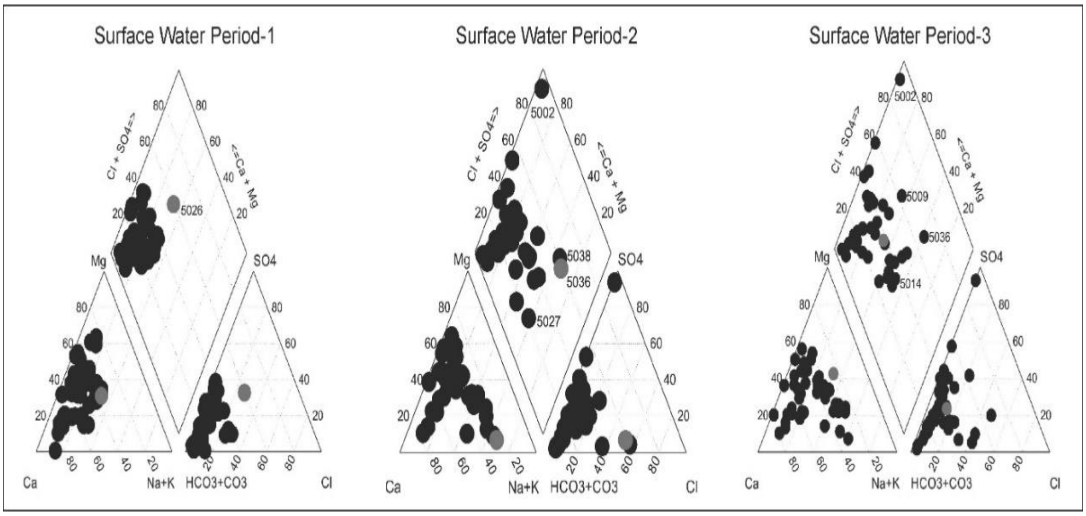

Figure 3.2 Piper diagrams of surface water samples sampled in three different periods in the Gediz graben (samples representing the whole Gediz Basin, not only Alaşehir sub-basin, modified from Eser Project, 2014)

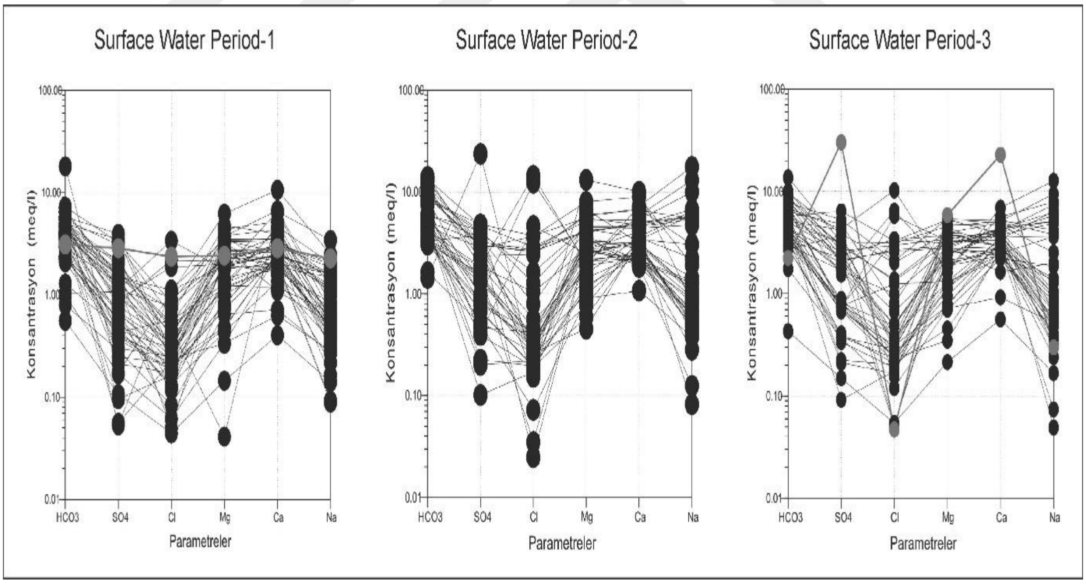

Figure 3.3 Schoeller diagrams of surface water samples sampled in three different periods in the Gediz Graben (samples representing the whole Gediz Basin, not only Alaşehir sub-basin**,** modified from Eser Project, 2014)

3.3.2 Groundwater

The Gediz Basin, which has a very complex hydrogeological structure, also shows a great variety in terms of groundwater water chemistry. Alluvial units, which spread over a wide area in the basin, have been enriched by ions Mg-Ca-HCO_3, Ca-Na-Mg-HCO_3, Na-Ca-Mg-HCO_3, Ca-Na-HCO_3, and Ca-Mg-HCO_3 (Figure 3.4 and Figure 3.5). The diversity of water types in the alluvium is associated with both water-rock interaction and anthropogenic effects. In the Gediz basin, volcanic rocks containing local groundwater have Ca-Mg-SO_4-HCO_3 water type, while Neogene limestones containing local groundwater have water type Ca-Mg-HCO_3. Waters from Palaeozoic units that crop out in the southern and northern parts of the basin have limited local groundwater and have Ca-Mg-HCO_3 (karstic) and Na-Ca-Mg-HCO_3 water types. Although calcium and magnesium cations dominate the waters coming from calc schists, sodium and calcium cations are more dominant in the waters coming from the areas where mica schists are located. The clastic units containing common groundwater around Alaşehir form a mixture with waters associated with both anthropogenic (such as agriculture) and geological processes (such as geothermal resources).

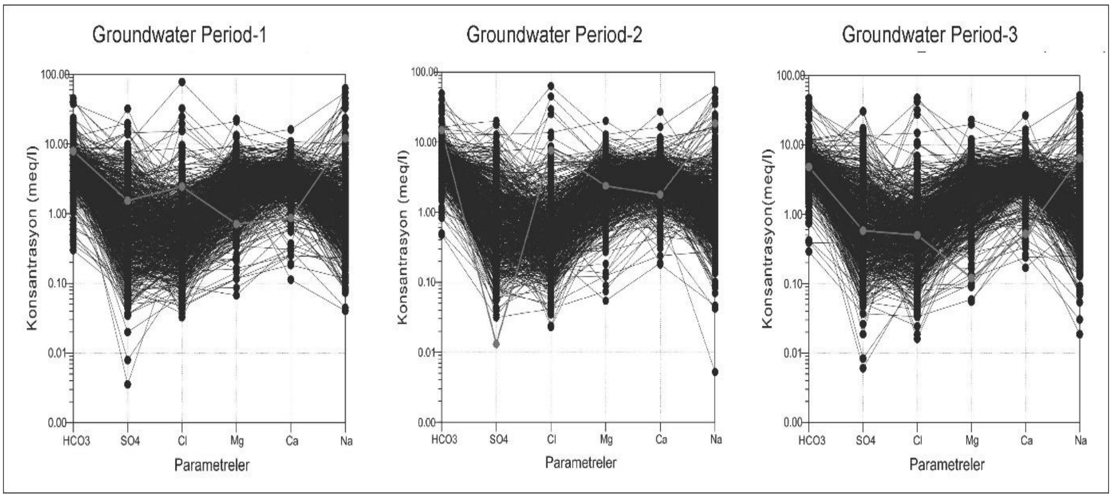

Figure 3.4 Schoeller diagrams of groundwater samples sampled in three different periods in the Gediz Graben (samples representing the whole Gediz Basin, not only Alaşehir sub-basin, modified from Eser Project, 2014)

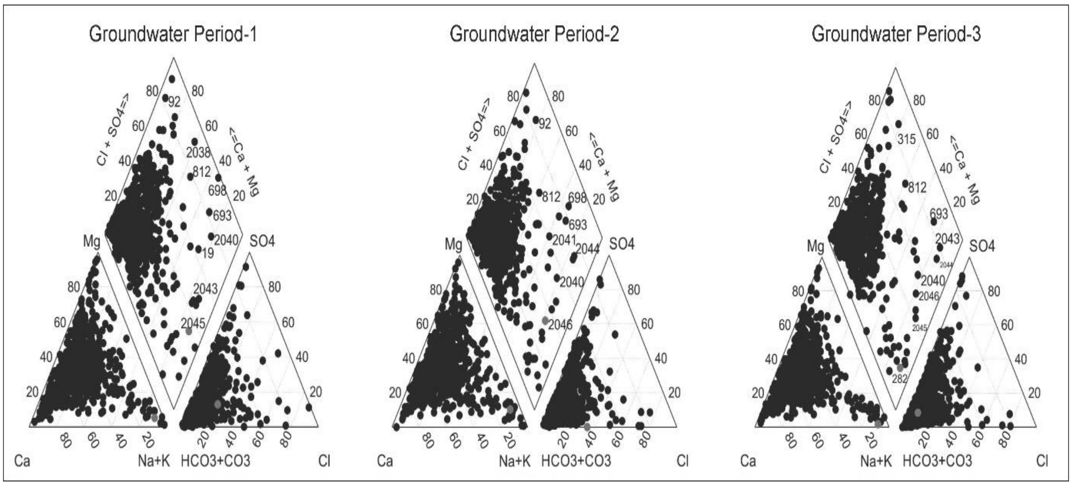

Figure 3.5 Piper diagrams of groundwater samples sampled in three different periods in the Gediz graben (samples representing the whole Gediz Basin, not only Alaşehir sub-basin, modified from Eser Project, 2014)

3.3.3 Geothermal Fluids

Geothermal fluid in Gediz Graben originates from structural controls related to the low angle Gediz detachment faults and high angle conjugate normal faults of Quaternary. Hydrogeochemical results (Uytun et al., 2020) showed that cold groundwater samples around the wells had high calcium and bicarbonate ions.

According to the Piper diagram (Figure 3.6), groundwater was characterized as Ca–HCO_3 type. This situation shows that the rocks from which these waters come are limestones and rocks containing carbonate. According to the Piper diagram (Figure 3.7), geothermal fluid samples shows rich characteristics of sodium and bicarbonate ions associated with metamorphic and Neogene sediments (schists, quartzites, granites, sandstones, and limestones). Most of the geothermal fluid from geothermal wells grouped under the Na-HCO_3 water type region of the Piper diagram. The rest of the samples are of mixed type and Na-Cl type. Generally, geothermal fluid concentrations of major ions were in the order of Na+K>Ca>Mg and HCO_3>Cl>SO_4. The reservoir rock chemistry was presumed to control the major ions of hot waters. As stated in previous studies (Rabet et al. 2017), Na^+ and K^+ concentrations in the geothermal fluid were very high compared to the cold groundwaters. A similar trend is seen in the Schoeller diagram (Figure 3.8), indicating that geothermal fluids have the same origin.

The Giggenbach Triangle (K-Mg-Na Triangle) representation allows you to verify the extent to which water-rock equilibrium has been attained (Giggenbach, 1988). The triangle is comprised of three zones: Immature waters (at the base); Partially equilibrated waters (in the middle); and Fully equilibrated waters (along the curve). Giggenbach diagram shows that -rock interaction has not reached mature water level, so this interaction is still in progress. Most of the samples are partially equilibrated waters and the rest of them are located on the bottom of the diagram, immature waters (Figure 3.7). This is a normal reflection due to graben-scale rock–water interaction. Immature meteoric waters enter a cycle through faults, infiltrating deep in the geothermal system, warming up, and rising to the surface. Fluid in existing reservoirs dynamically takes place in the geothermal system without sufficiently exposed to water-rock interaction.

One of the most important problems encountered in geothermal wells is scaling. Scaling occurs when certain elements in hot water reach saturation under certain conditions and then precipitate to form minerals and compounds (such as carbonate and silica). Saturation indexes from the chemical analysis can give us some ideas. When the samples taken from actively used wells are examined.

Example Field A from Alaşehir Graben: it is seen that the geothermal fluid is not saturated with anhydrite, aragonite, chalcedony, quartz, and gypsum minerals but is saturated with dolomite and calcite minerals. While Langelier has only scale-forming properties up to 60 °C depending on the temperature loss in saturation index values, it is scale-forming and corrosive at lower temperatures (Orakçı et al., 2019).

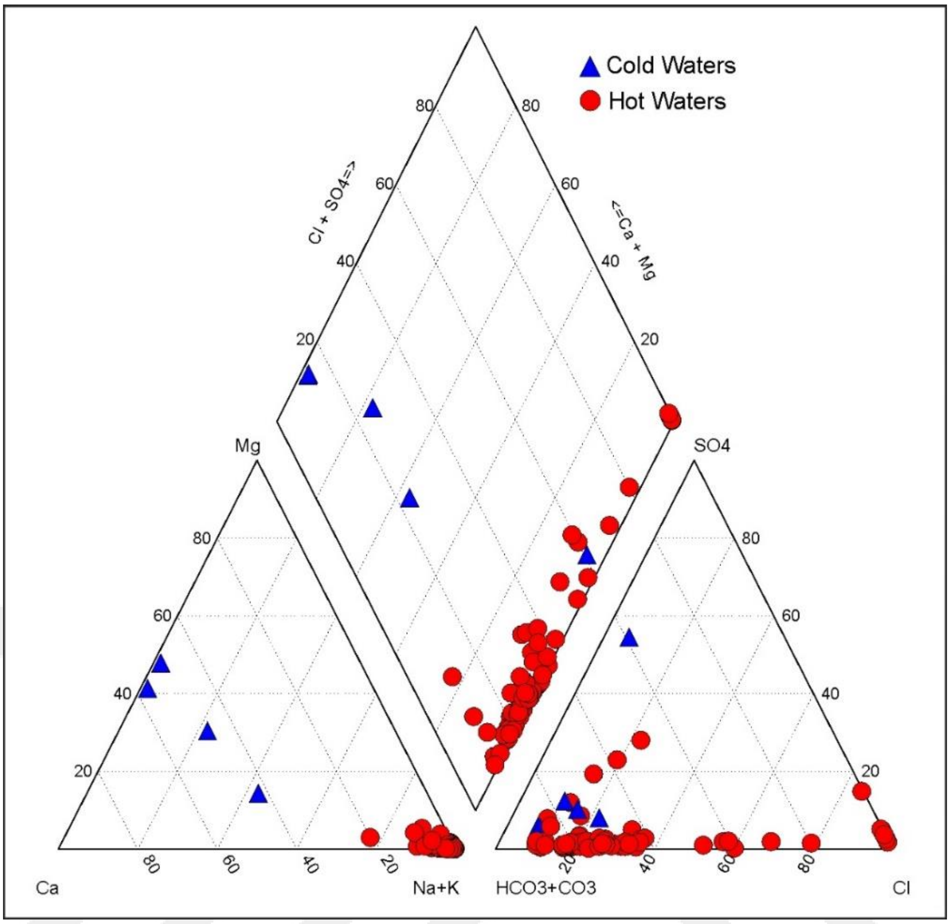

Figure 3.6 Piper diagram of cold water and geothermal fluid samples from the study area (modified from Eser Project, 2014)

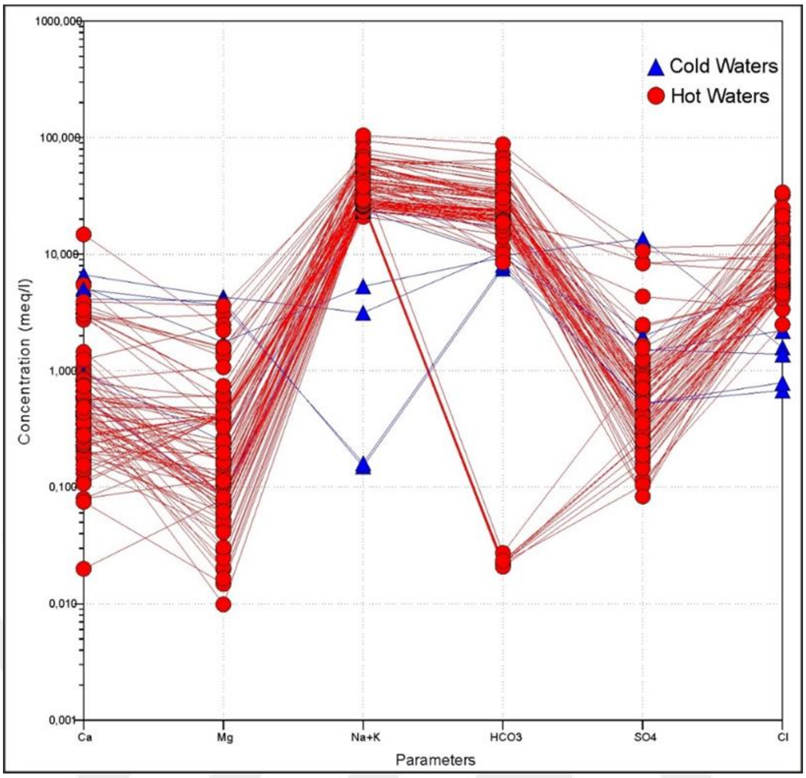

Figure 3.7 Schoeller diagram of cold water and geothermal fluid samples from the study area (modified from Eser Project, 2014)

Example Field B from Alaşehir Graben: Well group 1: It is seen that the geothermal fluid is not saturated with anhydrite and gypsum minerals but is saturated with calcedony, quartz, aragonite, talc, dolomite, and calcite minerals. Well group 2: It is seen that the geothermal fluid is not saturated with anhydrite, aragonite, calcite, dolomite, and gypsum minerals, but is saturated with calcedony and quartz minerals. Well group 3: It is seen that the geothermal fluid is not saturated with anhydrite, dolomite and gypsum minerals but is saturated with calcedony, quartz, aragonite, talc and calcite minerals (Orakcı et al., 2019).

According to the results of the saturation index, it is likely that chalcedony and quartz saturation may cause clogging in cracks, especially in reinjection wells, while saturation of calcite, aragonite and dolomite will cause scaling in production and transmission lines. It has been determined that lowering the temperatures up to 50 °C will provide saturation only with chalcedony and quartz, silica minerals.

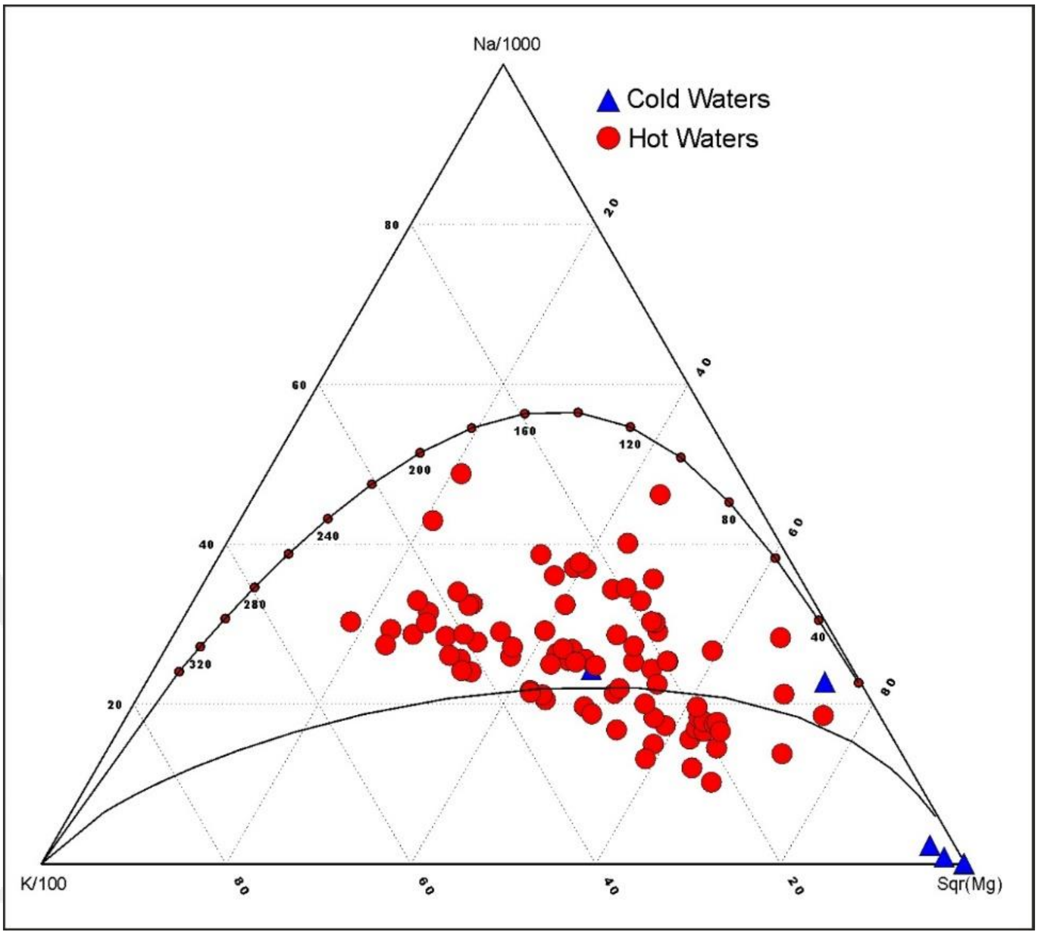

Figure 3.8 Distribution of the samples from Alaşehir sub-basin in the NaK-Mg1/2 triangular diagram (Giggenbach, 1988)

The geothermal fluid obtained from the wells in the field brings about 0.15-0.30 mmol/L $CaCO_3$ to the surface. According to geothermometer calculations, geothermal fluid has a carrying capacity of 1.0-1.6 mmol/L $CaCO_3$. Hot waters are saturated due to their high gas content, and most of the $CaCO_3$ is deposited in the reservoir and casings. Metal silicate scaling is not in question if the fluid temperature does not fall below 75° C degrees in the plant components.

In addition, there may be more scaling in the wells due to the high gas content of the fluid and the two-phase liquid around 500-700 meters. Uncondensed gas concentrations in the geothermal fluid are respectively CO_2, H_2S, CH_4, N_2, and H_2. The gas concentration determined in aquifers in the field reservoir is about 2% by weight.

Approximately 98-99% of the released gas (wt% in dry gas) is CO_2. In addition, since the separation pressure of the fluid produced from the power plant will be 15 bar and 170 degrees on average, there will be a 4-5% difference between the reservoir chemistry and reinjection water chemistry, although it varies from well to well due to steam loss.

CHAPTER FOUR

GEOTHERMAL ENERGY IN THE STUDY AREA

4.1 Geothermal Reservoir

The study area around Alaşehir in Gediz Graben is a crucial area for geothermal field development. Discovery of geothermal fluid in oil wells drilled in the region between 1999-2001 provided important information about the geothermal reservoir (Çiftçi, 2013). Geothermal activities in the study area gained momentum after the publication of the Geothermal Resources and Natural Mineral Water Law (No: 5686, Date: 3 June 2007) and the Implementation Regulation (No: 26727, Date: December 2007). The geology and geothermal potential of the region have been largely determined as a result of the drillings made by companies, most of which are in the private sector. Indirect use of geothermal energy is common in the study area. Looking at the field of study, it is seen that many different companies work in close neighbouring license fields and their wells are close to each other. This situation affects the production of geothermal wells and occasionally causes a conflict of interest. According to observations in the field, different companies produce and inject in the same geothermal reservoir.

In the Gediz Graben, geothermal systems were determined on a metamorphic basis. The geological units such as Alaşehir, Çaltılık, Gediz and Kaletepe Formations on the metamorphic basement act as cap rock. Menderes massif is composed of schists, quartzites, phyllites, and carbonates. Particularly, marble, schist, and mica schists are commonly observed in the reservoir. Besides marble and schists, calc-schist, dolomite gneiss, and quartzite are observed as well. Menderes Massif rocks are highly fractured due to faults, so that they are crucial considering geothermal operations. Geothermal fluid in Gediz Graben originates from structural zones of low angle Gediz detachment fault of Quaternary age and high angle normal faults of Holocene age. The geothermal fluid in the study area is of meteoric origin, and the reservoir fluid is liquid-dominated (Baba, 2015). For the geothermal application, many wells with the function of production and reinjection have been drilled with a depth range from 600 to 4300 m in the graben. Reservoir thickness Although the reservoir thickness varies in the study area, it can reach 1000 m. Reservoir thickness and temperature data are evaluated from drilling reports (Uytun et. al., 2020). There are medium-high enthalpy fields in the study area. Reservoir temperatures from geothermal wells at the southern part of the graben indicated high temperatures (>250°C). At the eastern part of the graben, reservoir temperatures are between 110-150°C (Figure 3.9). The maximum measured temperature is 287°C at the center of Gediz Graben. In the GRADIENT stage, reservoir temperatures estimates ranged from 193°C to 217° C based on quartz geothermometer. At the beginning of geothermal activities, wellhead pressures are measured around 50 bar (Table 1.1), while a decrease is observed over time. According to Aydın and Akın, the average reservoir pressure decline is estimated to be 3 bars per year (Aydın & Akın, 2021).

Figure 4.1 The uncontrolled flow of geothermal fluid from the well while the drilling process (Personal archive, 2011)

4.2 Geothermal Wells

There are 197 wells in total, 58 of which are reinjection wells drilled by the public and private sectors between 2002 and 2021 in the study area. These wells are belonging different companies and in different license areas. Some production wells very close to the reinjection wells. Almost all the reinjection wells reach the reservoir. Figure 4.1 shows a drilling rig in the study area. In this study, wells are classified as an injection, production, gradient, and out of use. In the study area, geothermal well depths vary between 600 and 4300. While shallow wells provide production from clastic units in fault zones, deep wells mainly receive hot water from units such as marble, mica-schist, quartz-schist, granite, granitic-gneiss, where fracture cracks systems in Menderes Massif improve secondary porosity and permeability. In Figure 4.3, drilling cuttings are seen from the Neogene levels in the study area. The table containing the temperature, flow rate, and coordinate information of the geothermal wells in the study area is given in Appendix-1. A summary table of the geothermal well data of the study area is given in the Table 1.1. The distribution of geothermal wells and geothermal power plants of the Alaşehir sub-basin is also shown in Figure 4.5. Flow rates of geothermal wells in the study area can reach up to 600-700 t / h. Although the capacities of the reinjection wells in the study area reach up to 600 t / h, they are generally around 200 t / h. The maximum temperature is 287º C measured in the MAK-14 well drilled by MTA and currently located in the license area of a private company. The map created from the well bottom temperatures of the geothermal wells in the study area is shown in Figure 4.4.

Table 1.1 Summary table of the geothermal well data of study area (Uytun et. al., 2020)

Well Type	Number	Depth Range	Well Bottom Temperature (°C)	Well Head Temperature (°C)	Flow (t/h)	Pressure (Barg)
Production	88	906-3945 m	128-287.5	80-287 °C	1-700	3-63
Reinjection	58	984-4312 m	102-263 °C	70-227 °C	7-660	1-53
Gradient& Other	51	400-3210 m	32-233 °C	29-213 °C	1-354	0.5-53

Figure 4.2 A drilling rig in the study area (Personal archive, 2011)

Figure 4.3 Drilling cuttings from Neogene levels in the study area (Personal archive, 2014)

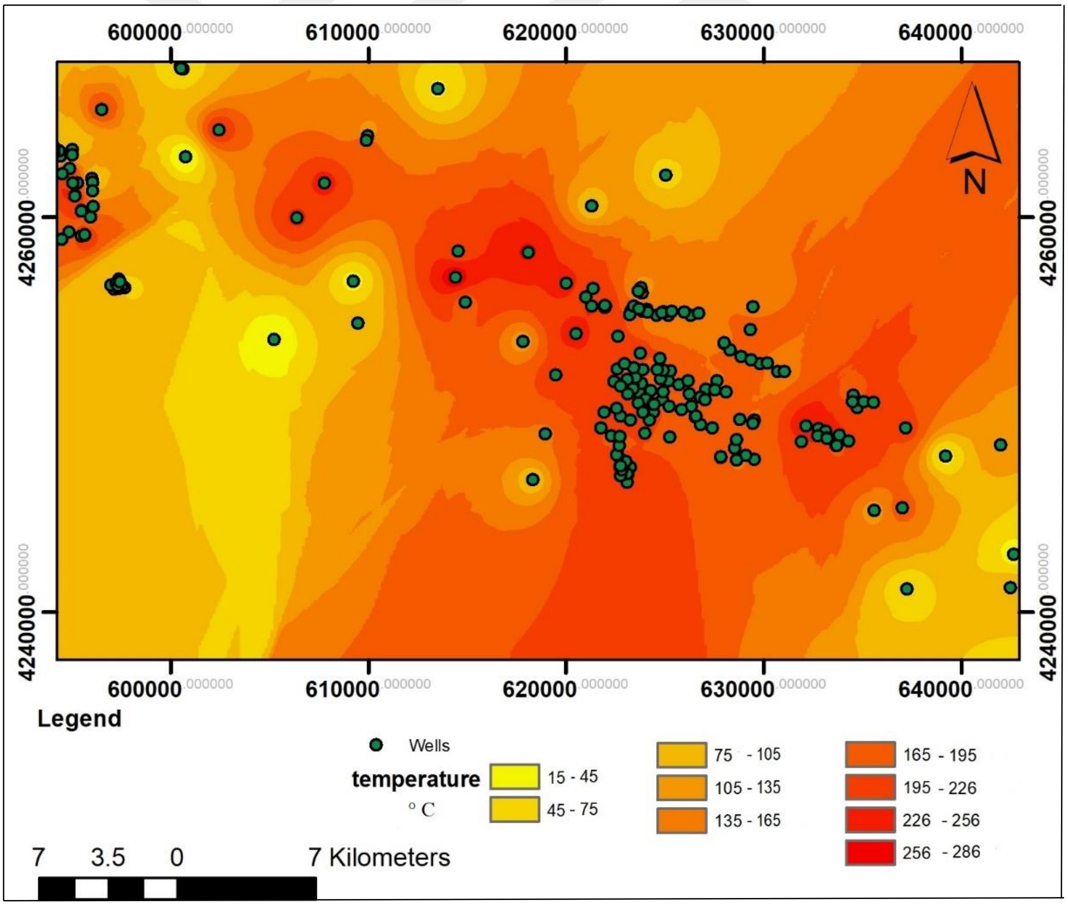

Figure 4.4 Bottomhole temperatures of the geothermal wells (Uytun et al., 2021)

4.3 Geothermal Power Plants in the Study Area

In the study area, there are 12 geothermal power plants owned by seven different firms with a total capacity of 308.92 MW (Table 4.1). One of them is a combined flash binary power plant, in other words, "hybrid", while the others are dual power plants. In addition to the completed geothermal power plants in the study area, there are also projects under the construction and GRADIENT phase. Although there are differences according to the projects, the power plants in the study area pay back their investments in an average of 10-12 years. Geothermal Licenses are issued to beneficiaries for a period of 30 years. At the end of 30 years, the process is extended for 10 years. Aydın & Akın reports that there are 7 different geothermal plant operators producing from the field with a total flow rate of 12650 tons per hour (Aydın & Akın, 2021). In addition to the existing investments, there are also projects carried out by domestic and foreign investors. With these investments, it is expected that the installed power in the working area will increase even more.

Table 4.1 Geothermal Power Plants (GPP) in the Alaşehir sub-basin (Uytun et al., 2021)

Geothermal Power Plant	Capacity (MW)	Operation Start Date	Geothermal Site
GPP-1	45	September 2015	Alkan - Şahyar
GPP-2	24	April 2016	Alkan-Piyadeler
GPP-3	24.9	May 2016	Kemaliye
GPP-4	24	October 2016	Alkan - Piyadeler
GPP-5	23.52	March 2017	Soğukyurt
GPP-6	10	June 2017	Örnekköy
GPP-7	19	July 2018	Baklacı
GPP-8	12	September 2018	Akkeçili
GPP-9	29.5	December 2018	Akkeçili - Baklacı
GPP-10	19	September 2019	Tepeköy
GPP-11	30	September 2019	Örnekköy
GPP-12	48	October 2019	Alkan

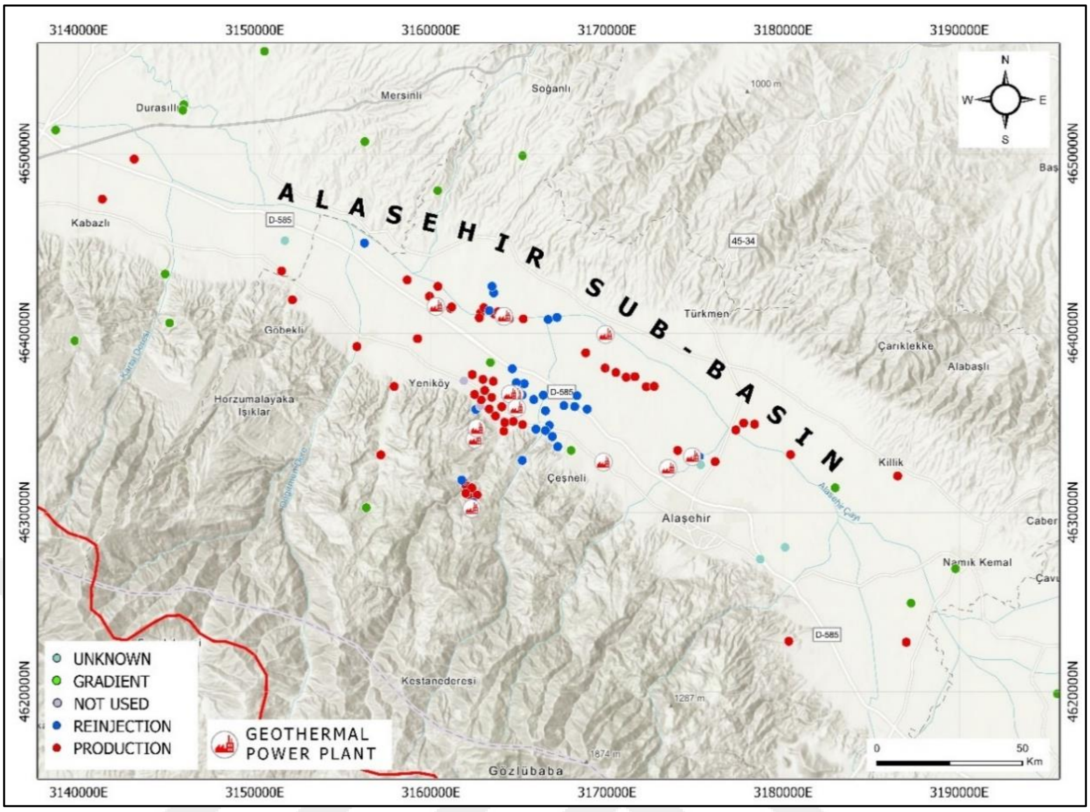

Figure 4.5 Geothermal wells and Geothermal Power Plants distribution of the Alaşehir sub-basin (Uytun et al., 2021)

Figure 4.6 A Geothermal Power in the study area (Personal archive, 2019)

CHAPTER FIVE

GEOTHERMAL ENERGY AND SEISMICITY IN THE GEDIZ GRABEN

5.1 Reservoir Geomechanics and Theoretical Background

The Aegean Region, which has undergone NS-oriented extensional deformation since the early Miocene period, is one of the most seismically active regions globally and has witnessed many devastating historical earthquakes (Arpat & Bingöl, 1969; Yılmaz, 2000; Sözbilir, 2001). Before the geothermal industrial activities began in Western Anatolia, devastating earthquakes occurred in the study area. The last major earthquake was the 1969 Alaşehir Earthquake (Arpat & Bingöl, 1969). Considering the seismic activity of the study area and the tectonic stress in the region, it may cause the faults to be reactivated due to geothermal activities. Therefore, it should be investigated and revealed whether geothermal activities trigger earthquakes in the study area.

As a concept set and approach, "reservoir geomechanics" aims to develop a solution to the problems that may occur during the life cycle of the reservoir by revealing the stress state of the reservoir in general. Developing a geomechanical model in a geothermal reservoir can help to understand future situations such as well failures, depletion, fault reactivation. A geomechanical model is closely related to all phases of work in a reservoir. According to Zoback, “the key component of a comprehensive geomechanical model is information on the current stress state (Zoback, 2007)”. In addition, zoback states that “there are three principal stress magnitudes, Sv, the vertical stress corresponding to the weight of overburden; S_{Hmax}, the maximum principal horizontal stress; and S_{Hmin}, the minimum horizontal stress” (Zoback, 2007). Anderson’s classification scheme defines stress relative magnitudes and orientations with respect to fault regime (see Figure 5.1). The definition of relative stress magnitudes and orientation is based on fault type. Andersen divided the faults into three groups in terms of their mechanical properties: normal fault, thrust fault, and strike-slip fault (Ketin & Canıtez, 1972). The current stress state is directly relevant to, pore pressure and tectonic regime. The stress state in the reservoirs can be estimated using various methods or measured by tests such as leak off and hydraulic fracturing in the field. Some wellbore imaging techniques such as ultrasonic televiewers is also used to estimate S_{Hmax}. Estimation of S_{Hmax} is very important for wellbore stability and the determination of optimal mud weight (Philippe, 2007). When designing the well, considering the stress correctly is very important for the stability of the well and preventing wellbore failures and sand production.

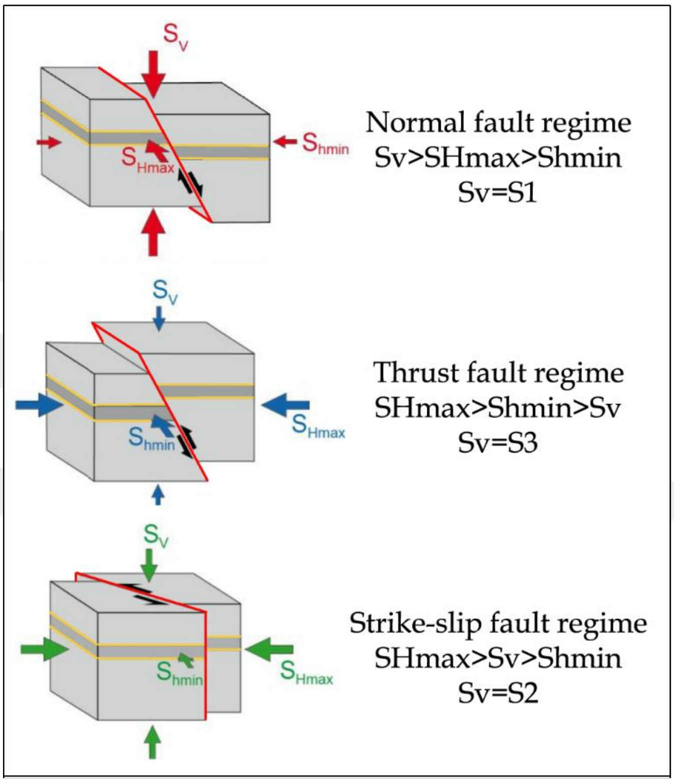

Figure 5.1 Fault types and stress regime categories (Anderson, 1905; Mariucci, 2020)

5.2 Present-day Stress Orientations and Magnitudes in the Gediz Graben

Various evaluations have been made about the direction and magnitude of stress in seismo-tectonic studies carried out in Gediz Graben (Kocyigit et al., 1999, Eyidogan & Jackson 1985; Kiratzi, 2002; Bozkurt and Sözbilir, 2004; Çiftçi & Bozkurt, 2009b). Even though these studies are helpful to understand the stress of the regime in general, they do not give comprehensive knowledge on the magnitudes of vertical, maximum horizontal, and minimum horizontal stress magnitudes. Çiftçi (2012) determines the present-day stress magnitudes in the Gediz Graben using data from multiple sources such as the existing field, earthquake data, and analyses of borehole failures data. According to Çiftçi (2012), stress magnitudes in Gediz Graben are as follows:

> The present-day stress field in the Gediz Graben is characterized by vertical maximum and horizontal 105º N-trending intermediate and 015ºN-trending minimum principal stress axes. Stress gradients are 23.4, 18.6, and 15.3 MPa/km for maximum, intermediate, and minimum stresses, respectively. This stress tensor aligns well with the observed fault pattern of the graben and confirms the~N-S-oriented extension. The strike\dip of optimum planes with the highest slip tendency is 105º\60ºS and 285º\60ºN, and the highest dilation tendency is on 105ºN-trending vertical fractures. Faults in the graben fill have near-normal frictional strength with a friction coefficient of (μ) 0.48. Pore pressure is generally hydrostatic, but local overpressure elevated to pore-fluid factor (λ) of 0.71 was observed in close proximity to the master bounding fault of the graben (Çiftçi, 2012).

Çiftçi (2012) reports that "Analysis of borehole breakouts using the four-arm caliper tool revealed 4 breakout intervals in Doğu Sarıkız-1 with a total length of 64.3 m. Along with these intervals, borehole enlargement is consistent in an NNE-SSW direction with an average orientation of 022º N." (see Figure 5.2). When maximum stress concentration exceeds the compressive rock strength, the borehole wall fails in compression, and pieces of wall rock spall off, resulting in borehole enlargement along the Shmin direction. This failure is called a wellbore breakout (Zoback, 1992; Bell, 1996; Çiftçi, 2012). Wellbore failures have an important role in understanding stress states.

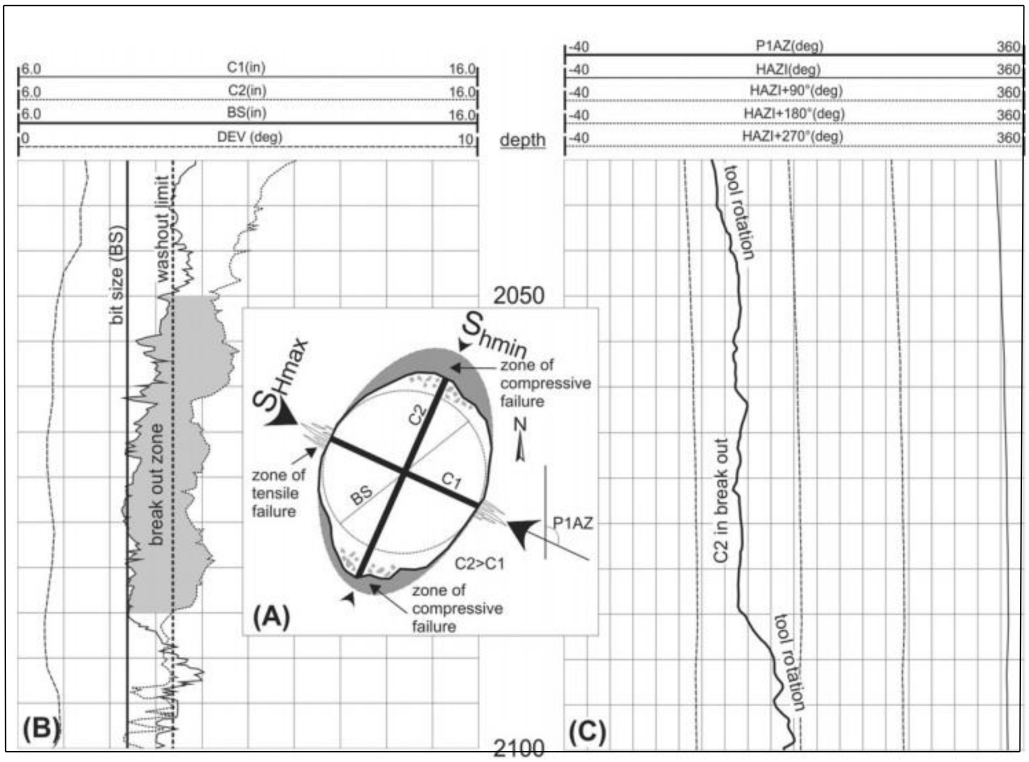

Figure 5.2 Descriptive example of well borehole breakouts in Doğu Sarıkız-1. (A) Breakouts occur due to compressive failure along the direction of minimum horizontal stress (Shmin), orthogonal to the maximum horizontal stress (SHmax). This results in enlargement of hole diameter and different caliper readings between C1 and C2. (B) Between 2050 and 2085 m, C2 caliper recorded consistently larger hole diameter due to breakout. (C) The azimuth of the C1 caliper (P1AZ) is constant in this interval and can be used to infer the orientation of breakouts along with C2 (Çiftçi, 2012)

5.3 Methods and Evaluation of Seismic Data

Production - reinjection data and seismic data were evaluated together with the tectonics and geology of the region by using the GIS software. In that analysis, especially seismicity was observed around geothermal wells drilled for reinjection (Appendix-2). It is concluded that earthquakes with magnitude 1-3 can be related to geothermal activity. However, no direct correlation was found between the pressure, flow rate, and the earthquake magnitude of the injected fluids (Figure 5.3 and Figure 5.4). No correlation was observed between the high pressures or flow reinjection and induced seismicity. In addition to the reinjection process, micro-earthquakes were observed during the hydraulic fracturing process, which may occur due to the reactivation of pre-existing faults. According to the Observatory - Earthquake

Research Institute and Prime Ministry Disaster and Emergency Management Presidency (AFAD) data, earthquake epicenter depths range between 2-10 km. Most of the earthquake epicenter depths are between 2-7 km intersecting Holocene and Quarternary fault zones and reservoir levels. Significant seismic activities observed at some locations are estimated to be related to Quarternary faults, which form the hottest regions (Figures 5.7). Geothermal fluids have been produced and injected in twelve different sites. Some of them interact with each other because they are so close to each other and the cause of seismicity is difficult to distinguish. These types of fields need to be studied in more detail.

Except for Kemaliye Geothermal Site, most of them are high-temperature fields. In general, high-temperature sites are seismically more active. It is anticipated that the high seismicity in high-temperature fields can be caused by active faults in these areas (Figure 5.6). The electricity generation of the Power Plants is taken from the website of the Turkish Energy Exchange Transparency Platform. Reinjection data is obtained from geothermal operators and Manisa Investment, Monitoring - Coordination Directorates. Although the research area has a background of natural seismicity, geothermal activities are thought to trigger earthquakes. It has been determined that 254 of the 302 earthquakes recorded between 1990-2020 in the study area took place between 2011-2020 (Figure 5.5). Most of the geothermal wells were drilled between 2011-2015 in the Gediz Graben. Fracturing operations and injection tests after drilling wells may have triggered seismicity. Although the seismicity decreases after the commencement dates of the power plants, it continues depending on the original conditions of the site, such as the proximity of the active faults. Before the geothermal fluid production and injection, the reservoir pressure of 5 MPa was reached locally at some locations. Reservoir pressure decreased to 1-2 MPa levels during geothermal application (Uytun et. al., 2020). This decline affected production and reinjection pressure in recent years. Flow rates and reinjection pressures fell drastically. The decrease in the reservoir pressure due to the change in the partial pressure of carbon dioxide also reduced the reinjection pressure. Since 2017, that decrease in reinjection pressure has caused a decrease in seismicity (Figure 5.5). As seen in Table 5.1 and Table 5.2, the great increase in the number of earthquakes in 2017 is thought to be the result of regional tectonic activity and geothermal activities working together. The fact that the reinjection pressures were higher and the installed capacity increased in these years supports this view (Figure 5.4). In addition, when an evaluation is made on a regional scale around the study area, it is striking that the number of earthquakes in 2017 was less than the number of earthquakes in the study area.

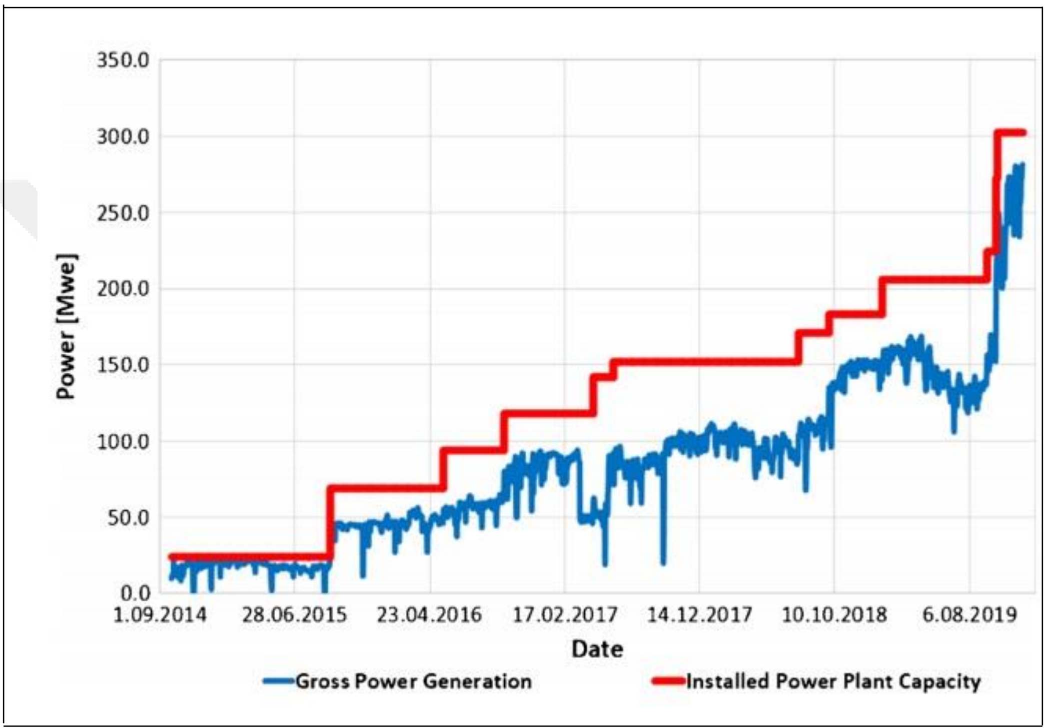

Figure 5.3 Installed power capacity and generated power (Aydın, 2021)

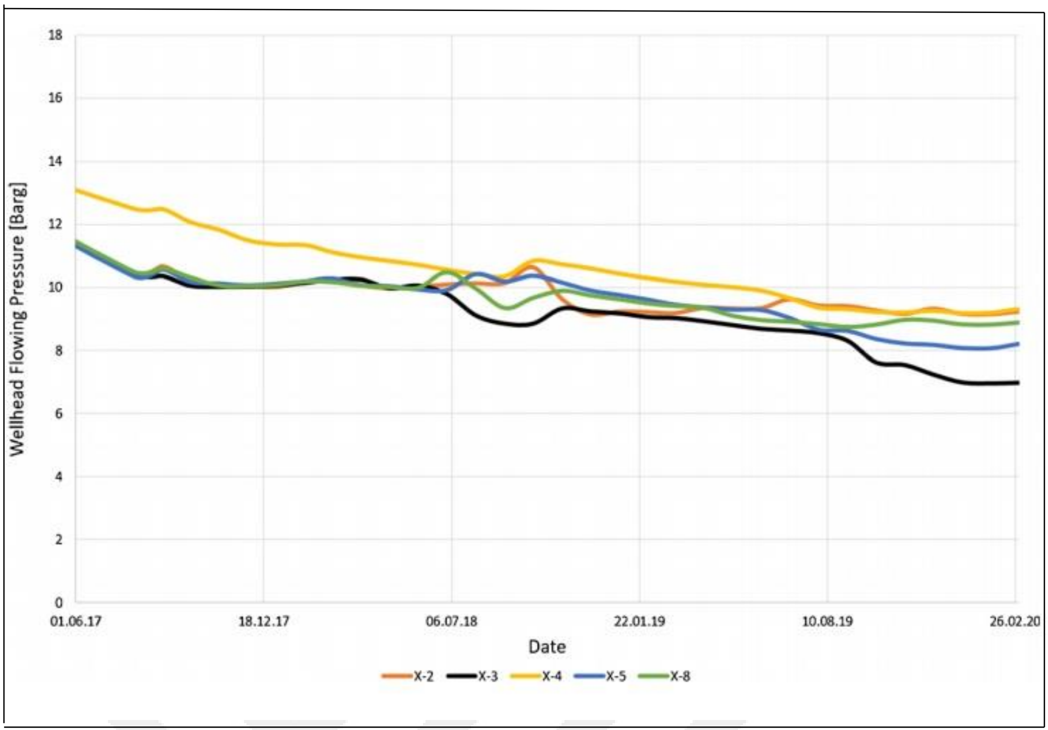

Figure 5.4 Wellhead flowing pressure of production wells located in the central field in Alaşehir, Turkey (Aydın, 2021)

Although the amount of production and reinjection is low, the most seismically active area is the Soğukyurt site. The maximum observed earthquake magnitude is 3.4 in the Soğukyurt site (Table 5.3). Soğukyurt reinjection site is on Gediz Graben Detachment Fault, and the metamorphic basement is cropped out at the surface (Figure 5.6). Minor seismicity is observed at the Alkan Piyadeler geothermal site. The maximum observed magnitudes are 2.2 at the Alkan Piyadeler and Şahyar- Çeşneli sites. Şahyar- Çeşneli site is more active than the Alkan-Piyadeler site seismically. Kemaliye and Örnekköy sites have minor seismicity, and the magnitudes are below 2. This data set points out that the induced seismicity may be related to the Gediz Graben Detachment Fault. For example, Soğukyurt geothermal field has minor reinjection capacity but also there is high seismicity observed (Table 5.3). The histogram of the observed earthquake magnitudes in the study area is depicted in Figure 5.5. Most of the magnitudes are ranging between 1 - 1.5 and 2 - 3. Other earthquakes are not related to geothermal fields, possibly due to different operating dates of the plant and reinjection wells.

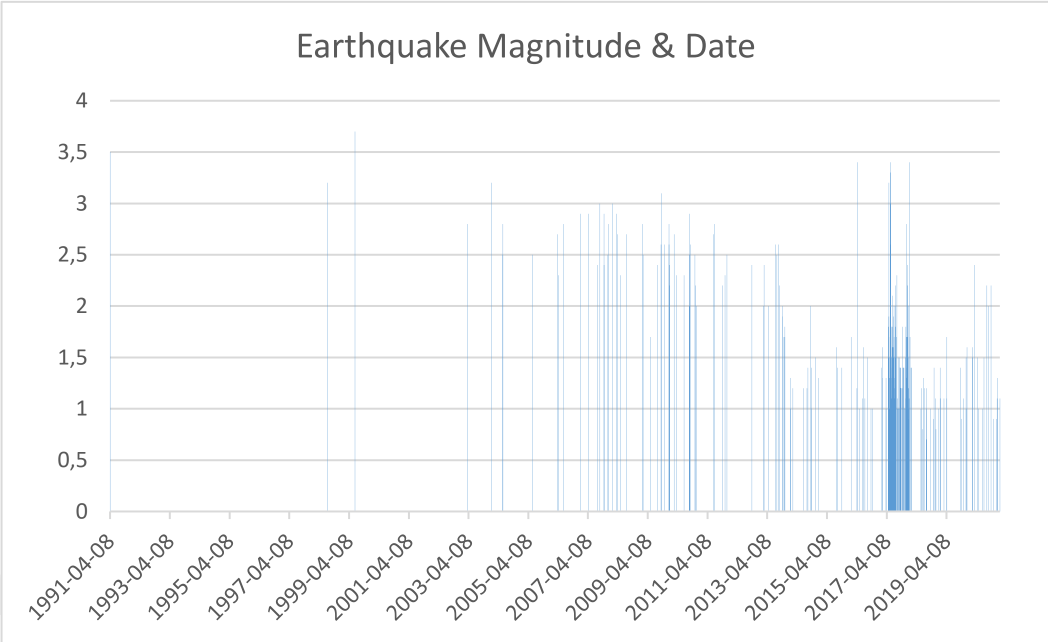

Figure 5.5 Observed earthquakes magnitudes in the Gediz Graben between 1990-2017 (Appendix-2)

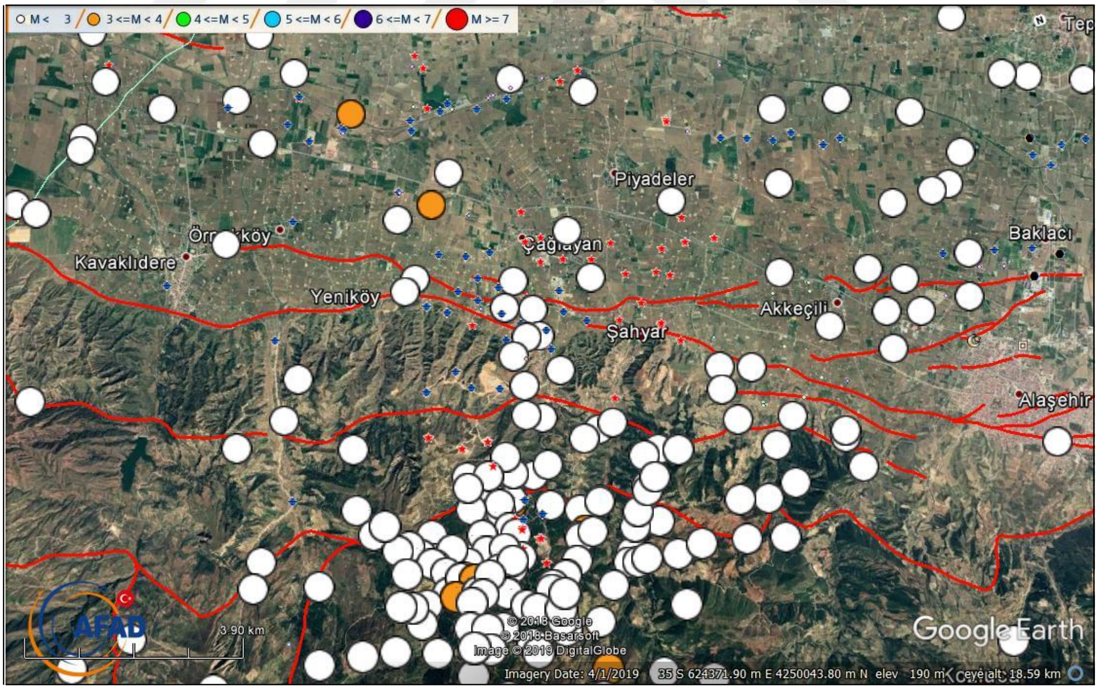

Figure 5.6 Earthquake epicenters (circles), geothermal wells (blue dots), reinjection wells (blue red stars), and active faults (red curves) (Uytun et al., 2021)

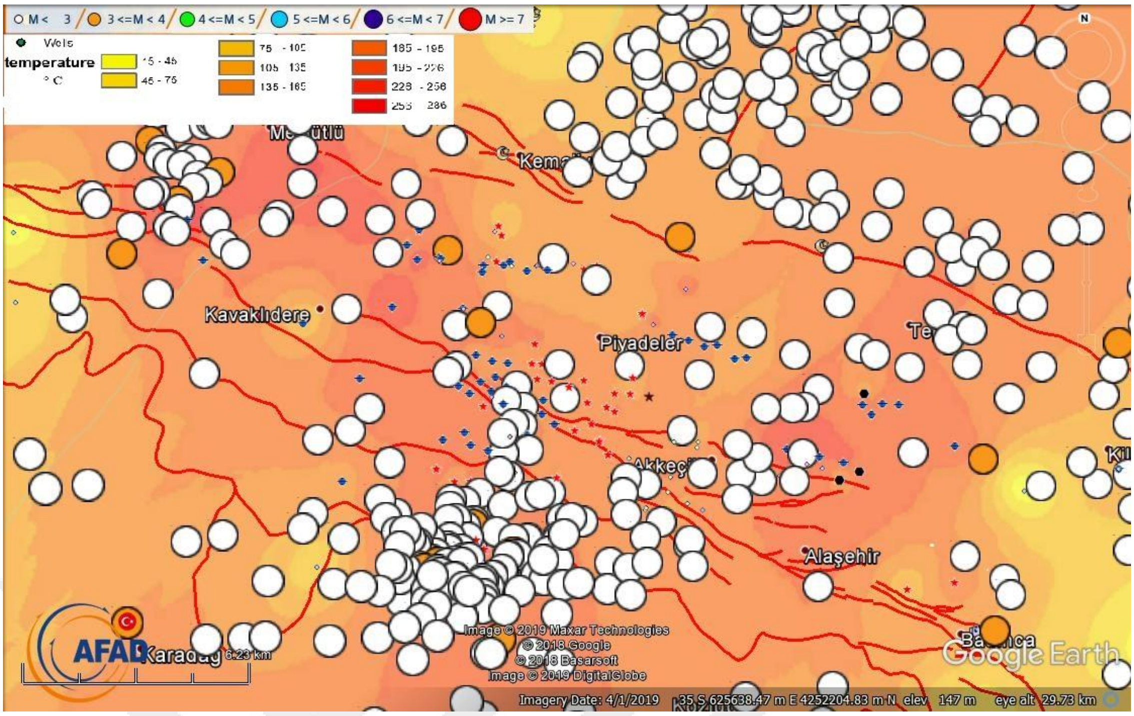

Figure 5.7 Earthquake epicenters, geothermal wells and bottomhole temperature (revised AFAD, 2021 & Uytun et al., 2021)

Table 5.1 Distribution of the number of earthquakes in the study area by years (AFAD, 2021)

Year	2020	2019	2018	2017	2016	2015	2014	2013	2012	2011	2010
Number of Earthquake	14	13	20	165	10	3	11	12	1	5	10
Year	2009	2008	2007	2006	2005	2004	2003	1999	1998	1991	
Number of Earthquake	11	5	8	3	1	3	1	1	1	1	

Table 5.2 Distribution of the number of earthquakes around 50 km of the study area by years (AFAD, 2021)

Year	2020	2019	2018	2017	2016	2015	2014	2013	2012	2011	2010
Number of Earthquake	63	55	87	453	72	68	121	161	54	84	175
Year	2009	2008	2007	2006	2005	2004	2003	1999	1998	1991	
Number of Earthquake	84	89	76	36	30	68	87	9	4	1	

Table 5.3 Geothermal sites and maximum observed magnitudes of earthquakes (Personal archive, 2021 & AFAD, 2021)

Power Plant	Capacity (MW)	Date of Operation Starting	Injection Depth [m]	Daily Average Injection (t / hour)	Seismicity	Largest Earthquake [ML, Md]	Reinjection Site	Geothermal Site
GPP-1	45	September 2015	1000-1900	2000	Moderate	2.2	Alaşehir Segment	Alkan - Şahyar
GPP-2	24	April 2016	1300-2700	1100	Minor	2.1	Alaşehir Segment	Alkan-Piyadeler
GPP-3	24.9	May 2016	700 - 3400	1700	Minor	1.4	Northern Graben Fault	Kemaliye
GPP-4	24	October 2016	1300-2700	1000	Minor	2	Alaşehir Segment	Alkan - Piyadeler
GPP-5	23.52	March 2017	1500-3700	800	Large	3.4	GG Detachment Fault	Soğukyurt
GPP-6	10	2017 June	2000-2500	550	Minor	1.6	Alaşehir Segment	Örnekköy
GPP-7	19	July 2018	2400-3000	550	Minor	1	Alaşehir Segment	Baklacı
GPP-8	12	September 2018	2100-2500	700	Minor	1.3	Alaşehir Segment	Akkeçili
GPP-9	29.5	December 2018	2400-3000	660	Minor	2.3	Alaşehir Segment	Akkeçili - Baklacı
GPP-10	19	September 2019	3170- 3900	800	Minor	1.3	Northern Graben Fault	Tepeköy
GPP-11	30	September 2019	2000-2400	1200	Minor	1.6	Alaşehir Segment	Örnekköy
GPP-12	48	October 2019	800-1200	1700	Minor	1.8	Alaşehir Segment	Alkan

CHAPTER SIX
CONCLUSION

A method called "traffic light system" has been used, especially in countries where enhanced geothermal system applications were conducted to trace production and reinjection activities. In worst-case situations, these activities in power plants can be halted using that method (Grigoli et al. 2017 & Gaucher 2018). Ensuring such kind of infrastructure concerning geothermal power plants in Western Anatolia is very important. The traffic light system is a unique method of controlling induced seismicity by simultaneously determining whether seismicity or associated risks have reached certain levels. It gives information about changing or stopping geothermal activities with green, yellow, orange, and red warning colours. Reducing injection or production rates, or potentially terminating the operation leads to a reduction in seismicity over time, but this can vary from hours to weeks. Depending on the seismicity level chosen in a traffic light system, imposing a warning and stopping operation when necessary will reduce the overall hazard and rsik of the project. After the danger has passed, the lights will turn green or yellow so that the operation can begin again (Walters et al., 2015; Bommer et al., 2006; Häring et al., 2008; Trutnevyte & Wiemer 2017).

Walters et al. also recommend what they call a case-specific traffic light system. Bommer et al. (2015) focus on estimating and mitigating risk rather than just induced seismicity hazard. The authors note that the success of induced seismic hazard control has not yet been proven and the focus is on insurance; structural they argue that measures should be taken, such as strengthening or relocating the population that has suffered damage from time to time. Wiemer et al. (2014) provide a list of recommendations for hazard and risk assessment, seismic monitoring, and traffic light systems that do not include an integrated system. Zoback (2007) proposes a five-step checklist for induced seismicity management: avoiding areas of active faults, installing stations for seismic monitoring, minimizing in-depth pore pressure changes, establishing modification protocols, and being prepared to change plans.

An example of geothermal-induced induced seismicity is the application in Basel, Switzerland. In 2006, in the Basel EGS project (5.0 km deep), earthquakes with a maximum magnitude of ML=3.4 occurred during the reservoir excitation and thousands of micro-seismicities required for the formation of the reservoir (Mena et al., 2013). Seismicity was felt widely in the city of Basel, with a population of 164,000, which was negatively received by both locals and the media. Claims for damages for the resulting damage reach 9 million dollars (Giardini, 2009; Edwards et al., 2015, Trutnevyte et al., 2017). Negative public reaction and subsequent risk updating the assessment (Baisch et al., 2009) led to the cancellation of the project. In 2013, St. Gallen hydrothermal project (4.5 km depth), induced earthquakes up to ML 3.5 magnitude have occurred (Wiemer et al., 2014; Edwards et al., 2015). Limited options to increase permeability due to insufficient water volume combined with a highly seismically sensitive fault zone, the St. Gallen project is over. The workflow chart of the traffic light system developed in Basel is shown in Figure 6.1.

The Riehen hydrothermal project (1.25 km injection, 1.55 km extraction depth) has been operating since 1989 without induced seismicity concerns; seismicity was not observed outside the region either (Evans et al., 2012). It is concluded that earthquakes with a magnitude of 1-3 can be related to geothermal activity. However, no direct correlation was found between the pressure, flow rate and the earthquake magnitude of the injected fluids. No correlation was observed between the high pressures or flow reinjection induced seismicity. In addition to the reinjection process, micro-earthquakes were observed during the hydraulic fracturing operations, which may occur due to the reactivation of pre-existing faults. In order to examine that incident in more detail, the seismometers should be deployed near to the power plants, and, following that, the change of the injection flow and pressure varying with time together with lithology should be determined.

Most of the earthquake epicenter depths are between 2-7 km intersecting Holocene - Quarternary fault zones and reservoir levels. Seismically most active locations may have a relation with the Quarternary faults which form the hottest regions.

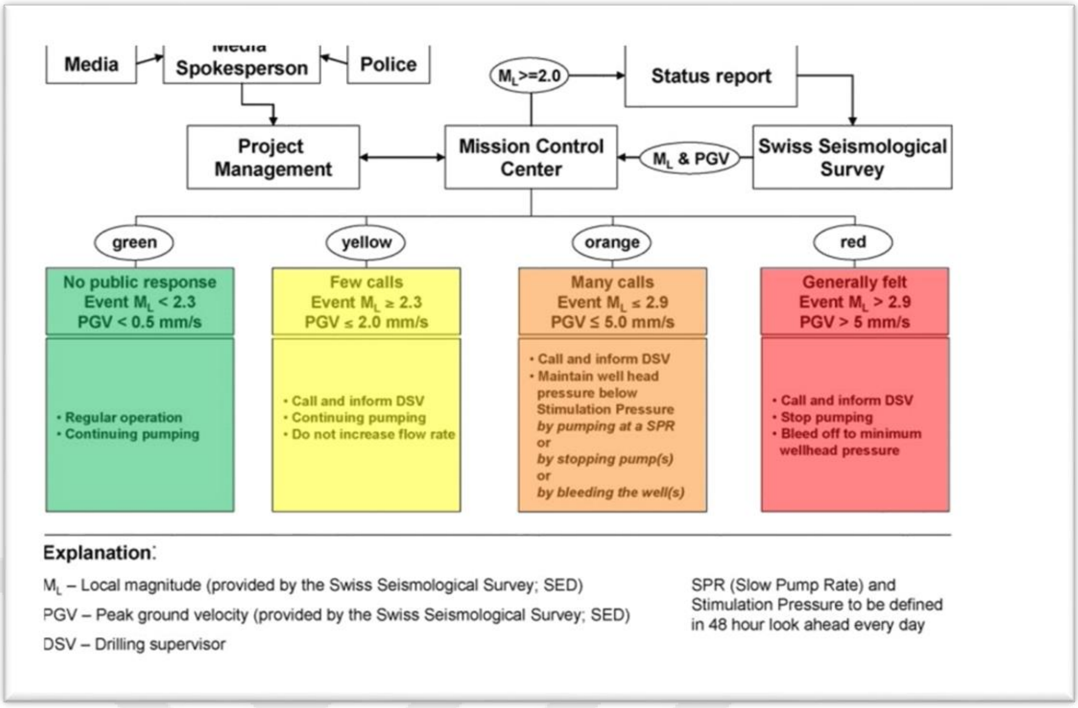

Figure 6.1 Trafic Light System in Basel (cited by Gauchner, 2015 and modified from Häring et al., 2008, Geothermics)

Progress of geothermal resources has been accelerated by releasing Law on Geothermal Resources and Natural Mineral Waters (No: 5686, Date: June 3, 2007) and its Implementation Regulation (No: 26727, Date: December 2007) in Turkey. Various environmental problems are experienced due to rapid development. Induced seismicity is also one of the neglected factors during that rapid development. Geothermal development is expected to be continued next years in Turkey, especially in the Gediz Graben. Therefore, methods should be developed to monitor the seismic effects of geothermal activities. Detailed studies can be then conducted to estimate the relationship between geothermal production-reinjection activities with seismicity. Additional, regional and local scale studies should be carried out to distinguish between induced and natural seismicity in the study area. It is necessary to monitor the stress change of the field to predict future problems such as compaction and induced seismicity in geothermal fields. Geomechanical modelling studies should be carried out in the geothermal field to understand the problems such as which type of wells will be drilled, what will be the highest injection pressure and stress distribution in the field.

This study was presented at the World Geothermal Congress (WGC 2020+1) and has taken its last updated form at the thesis stage after new findings and analyzes (Uytun et. al., 2021).

REFERENCES

Anderson, E. M. (1905). The dynamics of faulting. *Transactions of the Edinburgh. Geological Society, 8*, 387-402.

Arpat, E., & Bingöl, E. (1969). *Of the western Turkey; thoughts on its development.* Bulletin of the Mineral Research and GRADIENT , 73 (73). Retrieved May 15, 2021, from https://dergipark.org.tr/tr/pub/bulletinofmre/issue/3899/52028.

Aydin, H., & Akin, S., (2021). *Estimation of upcoming problems in Alaşehir geothermal field using a numerical reservoir model.* Retrieved May 16, 2021, from https://doi.org/10.1007/s12517-021-06830-z.

Baba, A. (2015). Application of geothermal energy and its environmental problems in Turkey. *International Journal of Global Environmental Issues*, *14*, 321–331.

Baba, A., & Ármannsson, H. (2006). Environmental impact of the utilization of geothermal area in Turkey. *Energy Source*, *1*, 267–278.

Baba, A., & Sözbilir, H. (2012). Source of arsenic-based on geological and hydrogeochemical properties of geothermal systems in western Turkey. *Chemical Geology*, *334*, 364-377.

Bell, J. S. (1996). In situ stress in sedimentary rocks (part 1): measurement techniques. *Geoscience Canada*, *23,* 85–100.

Bommer, J., Crowley, H., & Pinho, R. (2015). A risk-mitigation approach to the management of induced seismicity. *Journal of Seismol*ogy, *19*, 623-646.

Bozkurt, E. (2001). Neotectonics of Turkey – a synthesis. *Geodinamica Acta*, *14*, 3-30.

Bromley, C., & Majer, E. (2012). *Geothermal induced seismicity: risks and rewards.* Retrieved March 20, 2019 from https://www.researchgate.net/publication/258749472_Induced_Seismicity_Potential_of_Energy_Technologies.

Çiftçi, N. B. (2013). In-situ stress field and mechanics of fault reactivation in the Gediz graben, western Turkey. *Journal of Geodynamics, 65*, 136-147.

Çiftçi, N. B., & Bozkurt, E. (2009). Evolution of the miocene sedimentary fill of the Gediz graben, south west Turkey. *Sedimentary Geology, 216*, 49–79.

Davies, J. & Davies, D. Rhodri. (2010). Earth's surface heat flux. *Solid Earth*, *1*, 5-24.

Doglioni, C. (2018). *A classification of induced seismicity*. Retrieved June 20, 2020 from https://doi.org/10.1016/j.gsf.2017.11.015.

Edwards, B., Kraft, T., Cauzzi, C., Kästli, P., & Wiemer, S. (2015). Seismic monitoring and analysis of deep geothermal projects in St. Gallen and Basel, Switzerland. *Geophysical Journal International*, *201*, 1020-1037.

Emre, T. (1996). Geology and the tectonics of the Gediz Graben. *Turkish Journal of Earth Sciences*, *5*, 171-185.

Eser Mühendislik Müsavirlik A.Ş. (2014). Hydrogeological assessment of the Gediz watershed project report (Project Owner: DSI İzmir Regional Directorate, unpublished report).

Evans, K.F., Zappone, A., Kraft, T., Deichmann, N., & Moia, F. (2012). A survey of the induced seismic responses to fluid injection in geothermal and CO_2 reservoirs in Europe. *Geothermics, 41*, 30–54.

Giardini, D., 2009. Geothermal quake risks must be faced. *Nature*, *462*, 848–849.

Giggenbach, F. W. (1988). Geothermal solute equilibria. Derivation of Na-K-Mg-Ca geoindicators. *Geochimica et Cosmochimica Acta*, *52*, 2749-2765.

Grigoli, F., & Wiemer, S. (2017). *The challenges posed by induced seismicity*. Retrieved June 21, 2020 from https://doi.org/10.1029/ 2018EO074869.

Häring, M.O., Schanz, U., Ladner, F., & Dyer, B.C. (2008). Characterisation of the Basel enhanced geothermal system. *Geothermics, 5*, 469–495.

Hitzman, M. (2013). *Induced Seismicity Potential of Energy Technologies*. Retrieved December 20, 2020, from http://inducedearthquakes.org/.

Iztan, H., Harput, O.B., & Yazman, M. (1990). Geology of the Manisa region and hydrocarbon potential, Turkish Petroleum Corporation (TPAO) research group progress report no. 1592, Ankara, Turkey, unpublished report [in Turkish].

Jaeger, J., & G. W., Cook, N., & Zimmerman, R. (2007). *Fundamental of Rock Mechanics* (4th ed.). Wiley: Blackwell.

Karamanderesi, İ. H. & Yılmazer S. (1983). *Young tectonic movements and related geothermal energy possibilities in Gediz valley, Manisa*. Retrieved April 20, 2021 from http://digitallibrary.un.org/record/91703.

Karamanderesi, İ. H., Yılmazer, S., Yıldırım, T., Yakabağ, A., Çiçekli K., Gevrek, A. İ., Demir A., & Yıldırım, N. (1995). Gediz valley geothermal energy gradient survey and drilling (SC-1) data result report between Manisa-Turgutlu-Salihli-Alaşehir. MTA General Directorate, Report No:10460, Ankara (unpublished).

Ketin, İ., & Canıtez, N. (1972). *Structural geology* (2nd ed.). İstanbul: İTÜ.

Koçyiğit, A., Yusufoglu, H., & Bozkurt, E. (1999). Evidence from the Gediz graben for episodic two-stage extension in western Turkey. *Journal of the Geological Society, 156*, 605–616.

Koçyiğit, A., Unay, E., & Saraç, G. (2000). Episodic graben formation and extensional neotectonic regime in west central Anatolia and the Isparta angle: a case study in the Aksehir-Afyon graben, Turkey. *Geological Society*, *173*, 405-421.

Konietzky, H., & Yildizdag, K. (2018). *Geohydraulics – fundamentals.* Retrieved June 20, 2020 from https://tu-freiberg.de/fakult3/gt/feme/e-book/31_Geohydraulics-fundamentals.pdf.

Lehtonen, A., Cosgrove, J., Hudson, A. J., & Johansson, E. (2012). *An examination of in situ rock stress estimation using the Kaiser effect*. Engineering Geology, 124. Retrieved June 18, 2020 from https://doi.org/10.1029/ 2018EO074869.

McKenzie, D. (1978). Active tectonics of the Alpine—Himalayan belt: the Aegean sea and surrounding regions. *Geophysical Journal International*, *55*, 1, 217–254.

Mariucci, M.T., & Montone, P. (2020). *Database of Italian present-day stress indicators. IPSI* 1.4. *Sci Data* **7**, 298. Retrieved July 13, 2021 from https://doi.org/10.1038/s41597-020-00640-w.

McClure, M., & Horne, R. (2012). *The effect of fault zone development on induced seismicity*. 37th Workshop on Geothermal Reservoir Engineering, Stanford University, Stanford, California. Retrieved July 13, 2021 from https://pangea.stanford.edu/ERE/pdf/IGAstandart/SGW/2012/Mcclure.pdf.

Mena, B., Wiemer, S., & Bachmann, C. (2013). Building robust models to forecast the induced seismicity related to geothermal reservoir enhancement. *Bulletin of the Seismological Society of America, 103*, 383-393.

Orakcı, A., Doğdu, N., Akar, M., & Duran, Y. (2019). *Türkerler geothermal energy GRADIENT and production company revised resource protection areas study project for the area with operating license numbered Manisa alaşehir 2017/02 on behalf of.* 2018-33-47. MTA unpublished report [in Turkish].

Philippe, G., Brewer, T., Pezard, P., & En-Chao Y., (2007). *Borehole imaging tools principles and applications.* Scientific Drilling, 5 (5). Retrieved April 10, 2020 from https://publications.iodp.org/sd/05/suppl/Borehole_Imaging_Tools.pdf.

Rabet, R. S., Şimşek, C., Baba, A., & Murathan, A. (2017). Blowout mechanism of Alasehir (Turkey) geothermal field and its effects on groundwater chemistry. *Environ Earth Science,* (2017), 76-49.

Şengör, A.M.C., & Yılmaz, Y. (1981). Tethyan evolution of Turkey: a plate tectonic approach. *Tectonophysics*, *75*, 181-241.

Seyitoğlu, G., & Işik V. (2015). Late cenozoic extensional tectonics in western Anatolia: exhumation of the Menderes core complex and formation of related basins. *MTA Dergisi*, *151*, 49-109.

Seyitoğlu, G., & Scott, B.C. (1996). The age of Alaşehir graben (west Turkey) and its tectonic implications. *Geology Journal*, *31*, 1−11.

Seyitoğlu, G., Çemen, I., & Tekeli, O. (2000). Extensional folding in the Alaşehir Gediz graben, western Turkey. *Journal of the Geological Society*, *157*, 1097–1100.

Sözbilir, H. (2001). Geometry of macroscopic structures with their relations to the extensional tectonics: field evidence from the Gediz detachment, western Turkey, *Turkish Journal of Earth Sciences*, *10*, 51-67.

Sözbilir, H. (2002). Geometry and origin of folding in the Neogene sediments of the Gediz graben, western Anatolia, Turkey, *Geodinamica Acta*, *15*, 277−288.

Sözbilir, H., & Emre T. (2007). Tectonic evolution of the Kiraz basin, Küçük Menderes graben: evidence for compression/uplift-related basin formation overprinted by extensional tectonics in west Anatolia. *Turkish Journal of Earth Sciences 16*, 441-470.

Özkaymak, Ç. & Sözbilir, H. (2008). Stratigraphic and structural evidence for fault reactivation: the active Manisa fault zone, western Anatolia . *Turkish Journal of Earth Sciences* , *17* (3) , 615-635.

Tarcan, G., Filiz, Ş., & Gemici, U. (2000). *Geology and geochemistry of the Salihli geothermal fields, Turkey.* Retrieved April 11, 2020 from https://geothermal-energy.org/pdf/IGAstandart/WGC 2000/issue/R0922.PDF

Trutnevyte, E., & Wiemer, S. (2017). Tailor-made risk governance for induced seismicity of geothermal energy projects: An application to Switzerland. *Geothermics, 65*. 295–312.

Walters, R. J., Zoback, M., Baker, J.W., & Beroza, G.C. (2015). Characterizing and responding to seismic risk associated with earthquakes potentially triggered by fluid disposal and hydraulic fracturing. *Seismological Research Letters*, *86*, 1110–1118.

Wiemer, S., Kraft, T., & Landtwing, D. (2014). *Energy from the earth: deep geothermal as a resource for the future? Swiss Geothermal Project Final Report.* Paul Scherrer Institute, Villigen.

Uytun, H., Deniz, V., & Özkan L. (2020). *Manisa province geothermal energy potential update report*. Manisa Govermentship (unpublished report).

Uytun, H., Baba, A., Sözbilir, H., Yıldızdağ, K. & Karaş, M. (2021). *Relation between induced seismicity and geothermal systems: a case study from the Gediz graben, western Anatolia, Turkey*. World Geothermal Congress 2020+1, Reykjavik, Iceland. Retrieved July 11, 2021 from https://pangea.stanford.edu/ERE/db/WGC/papers/WGC /2020/13228.PDF

Uzel, B., Sozbilir, H., Özkaymak, Ç., & Kaymakçı, N., & Langereis, C. (2013). Structural evidence for strike-slip deformation in the Izmir–Balıkesir transfer zone and consequences for late cenozoic evolution of western Anatolia (Turkey). *Journal of Geodynamics, 65*, 94-116.

Yılmaz, Y. (2000). Active tectonics of the Aegean region. *Symposium on Seismicity of Western Anatolia*. İzmir: Chamber of Geological Engineers.

Zang, A., Oye, V., Jousset, P., Deichmann, N., Gritto, R., McGarr, A., Majer, E., & Bruhn, D. (2014). Analysis of induced seismicity in geothermal reservoirs – An overview. *Geothermics*, *52*, 6-21.

Zoback, M. D., (2007). *Reservoir Geomechanics* (3^{rd} ed.). New York: Cambridge University Press.

Zoback, M. L., (1992). First- and second-order patterns of stress in the lithosphere: the world stress map project. *Journal of Geophysical Research, 97*, 11703–11728.

APPENDICES

Appendix-1

Table A1 Seismic data of the study area (AFAD, 2021)

No	EventID	Agency	Tarih(UTC)	Latitude	Longitude	Depth	Rms	Type	Magnitude
1	494988	AFAD	2021-02-05 10:48:12	38.6001	28.0471	7.27	0.45	ML	1.9
2	494705	AFAD	2021-02-02 13:41:23	38.866	28.5468	7	0.38	ML	1.1
3	494567	AFAD	2021-02-01 13:48:24	38.2171	28.3211	10.49	0.53	ML	1.9
4	494347	AFAD	2021-01-29 01:57:46	38.535	28.1881	7.02	0.55	ML	1.8
5	494343	AFAD	2021-01-28 22:43:25	38.5918	28.1941	7.01	0.31	ML	1.5
6	494139	AFAD	2021-01-25 08:06:32	38.3855	28062	7	0.61	ML	2.4
7	493852	AFAD	2021-01-21 08:17:25	38.3021	28.0626	7	0.27	ML	0.7
8	493740	AFAD	2021-01-19 21:03:41	38.2876	28.0905	7	0.48	ML	1.3
9	493707	AFAD	2021-01-19 09:28:21	38.3905	28.688	6.93	0.36	ML	1.1
10	493392	AFAD	2021-01-13 11:28:45	38.4543	28.6043	3.12	0.35	ML	1.2
11	492947	AFAD	2021-01-07 04:14:28	38.4683	28.1003	7.09	0.53	ML	2
12	492840	AFAD	2021-01-05 12:08:04	38.7196	28.2471	7	0.28	ML	1.1
13	491894	AFAD	2020-12-26 09:54:59	38.5511	28.6278	10.64	0.59	ML	1.3
14	491893	AFAD	2020-12-26 09:31:37	38.5671	28.5198	7.59	0.39	ML	1
15	491840	AFAD	2020-12-25 16:35:01	38.0388	28.5048	7	0.21	ML	1
16	491786	AFAD	2020-12-24 13:18:50	38.299	28.6143	7	0.2	ML	1.3
17	491045	AFAD	2020-12-15 22:46:11	38.4341	28.631	10.13	0.17	ML	1.1
18	490733	AFAD	2020-12-12 08:05:03	38.2733	28.7023	9.7	0.56	ML	1.3
19	490063	AFAD	2020-12-04 07:56:31	38.4328	28.3843	7	0.39	ML	0.9
20	489386	AFAD	2020-11-27 23:50:27	38.2251	28.7888	7	0.16	ML	1.1
21	488735	AFAD	2020-11-21 12:27:37	38.7005	28.2136	7.04	0.22	ML	1.3
22	488602	AFAD	2020-11-20 15:13:35	38.3741	27.8858	7	0.69	ML	1.2
23	488264	AFAD	2020-11-17 07:07:00	38.5458	28.1808	7.01	0.42	ML	1.3
24	487773	AFAD	2020-11-13 11:09:46	38.365	28092	7	0.52	ML	1
25	487769	AFAD	2020-11-13 10:23:35	38.3746	28.1215	7	0.22	ML	1
26	487566	AFAD	2020-11-12 05:33:30	38.3523	28.1138	7.06	0.71	ML	1.2
27	483718	AFAD	2020-10-29 04:09:52	38.329	28.3248	7	0.41	ML	0.9
28	483643	AFAD	2020-10-27 18:00:41	38.3738	27.9973	7	0.53	ML	1.4
29	482168	AFAD	2020-10-17 13:15:07	38.2693	27.9451	7.04	0.27	ML	1.8

Table A1 continues

30	481516	AFAD	2020-10-05 15:52:58	38.141	28.1798	7	0.38	ML	0.9
31	481454	AFAD	2020-10-03 12:56:15	38.108	28.1838	7	0.51	ML	1
32	481426	AFAD	2020-10-03 03:43:57	38.4273	28.4353	5.31	0.35	ML	2.2
33	481389	AFAD	2020-10-02 19:50:15	38.2118	28.8368	7	0.5	ML	1.1
34	481166	AFAD	2020-09-28 19:57:41	38.2088	28.2511	7	0.53	ML	1.1
35	480719	AFAD	2020-09-20 20:49:51	38.6706	27.9651	6.78	0.39	ML	0.9
36	480178	AFAD	2020-09-10 17:51:14	38.5716	28.1096	7.04	0.53	ML	1.8
37	479699	AFAD	2020-08-31 12:20:21	38.5745	28.0088	7	0.69	ML	1.1
38	479481	AFAD	2020-08-28 00:59:52	38.401	28.3993	6.9	0.22	ML	2
39	479418	AFAD	2020-08-26 11:30:15	38.7045	28.2256	7	0.17	ML	1.1
40	479164	AFAD	2020-08-20 06:00:19	38.565	28.2056	7	0.37	ML	1.2
41	478968	AFAD	2020-08-14 19:31:30	38.7021	28.0198	9.34	0.8	ML	1.5
42	478859	AFAD	2020-08-12 19:31:24	38.3945	28.5393	7.11	0.32	ML	2.2
43	477962	AFAD	2020-07-24 12:45:24	38.6475	28193	6.87	0.3	ML	0.8
44	477359	AFAD	2020-07-11 21:45:33	38.1478	28.8395	7.1	0.65	ML	1.1
45	477084	AFAD	2020-07-06 20:44:59	38.3753	28.5253	7.09	0.48	ML	1.5
46	476609	AFAD	2020-06-27 09:50:45	38.4876	28.6196	24.58	0.13	ML	1
47	476312	AFAD	2020-06-22 12:33:22	38.4438	28.5888	29.81	0.35	ML	1
48	474880	AFAD	2020-06-01 04:20:13	38.6833	28.0016	9.25	0.8	ML	1.1
49	474056	AFAD	2020-05-20 13:04:18	38.314	28.8773	7	0.41	ML	1
50	472990	AFAD	2020-05-03 22:26:24	38.3416	28.2811	7	0.4	ML	1
51	471965	AFAD	2020-04-20 17:16:47	38.2643	28.6188	7	0.57	ML	1.5
52	471441	AFAD	2020-04-13 05:46:26	38.1886	28862	7	0.34	ML	1.9
53	471434	AFAD	2020-04-13 05:18:15	38.1655	28.8491	10.47	0.26	ML	2.9
54	471124	AFAD	2020-04-09 05:35:40	38.1816	28.8843	7	0.5	ML	1.2
55	471125	AFAD	2020-04-09 05:35:22	38.2	28874	7	0.42	ML	1.2
56	471017	AFAD	2020-04-07 16:09:39	38.1726	28.8398	7.01	0.35	ML	2.3
57	471015	AFAD	2020-04-07 15:51:43	38.1655	28.8595	6.99	0.26	ML	2.2
58	471014	AFAD	2020-04-07 15:50:01	38.172	28.8476	10.24	0.34	ML	2.3
59	471008	AFAD	2020-04-07 12:25:34	38.1826	28868	7	0.34	ML	1.5
60	471006	AFAD	2020-04-07 11:56:27	38.1736	28.8663	7.82	0.29	ML	2.6
61	470900	AFAD	2020-04-05 19:38:18	38.2686	28312	7	0.19	ML	2.7
62	469381	AFAD	2020-03-16 15:01:36	38.3698	28.3951	7.01	0.28	ML	2.4

Table A1 continues

63	468703	AFAD	2020-03-08 04:43:47	38.2756	28.2568	7	0.16	ML	1.4
64	468601	AFAD	2020-03-06 22:47:19	38.3525	28153	7	0.7	ML	1.5
65	468197	AFAD	2020-03-03 13:41:46	38.2168	28.7051	7	0.29	ML	1.5
66	467548	AFAD	2020-02-26 23:45:02	38.3121	28.7116	7	0.24	ML	1
67	466401	AFAD	2020-02-22 09:42:10	38.4038	28.5471	11.15	0.68	ML	1.5
68	466081	AFAD	2020-02-20 07:44:11	38.1465	28.1781	7	0.54	ML	1
69	465609	AFAD	2020-02-18 12:21:03	38.2655	28.5281	7	0.38	ML	1.6
70	464864	AFAD	2020-02-13 11:01:56	38.1661	28.0671	6.75	0.47	ML	1.1
71	462048	AFAD	2020-01-31 19:46:32	38.513	27.9625	7	0.16	ML	1
72	462008	AFAD	2020-01-31 17:36:25	38.5983	27.8981	7	0.43	ML	1.6
73	457326	AFAD	2020-01-23 07:33:15	38.7821	28.1453	7.76	0.36	ML	2.4
74	456328	AFAD	2020-01-10 02:46:44	38.5573	28.2453	6.99	0.59	ML	1.5
75	456204	AFAD	2020-01-07 20:42:39	38.6605	27.9416	7	0.37	ML	1.9
76	455461	AFAD	2019-12-25 04:42:31	38.6295	28.0335	7.08	0.22	ML	1.2
77	454147	AFAD	2019-12-15 04:02:15	38.2968	28.3721	7	0.49	ML	1.6
78	453631	AFAD	2019-12-08 11:38:53	38.2806	28.7645	7	0.49	ML	1.3
79	453268	AFAD	2019-12-01 09:44:15	38.3186	28.3386	5.55	0.55	ML	1.5
80	453269	AFAD	2019-12-01 09:38:37	38.3116	28.3265	7	0.49	ML	1
81	453270	AFAD	2019-12-01 09:36:16	38.315	28.3813	7	0.47	ML	1
82	451919	AFAD	2019-11-06 01:43:59	38.517	28.2036	6.97	0.66	ML	1.7
83	450933	AFAD	2019-11-04 22:57:54	38.3565	28.5081	7	0.31	ML	1.1
84	450750	AFAD	2019-11-01 17:39:06	38.613	28.4555	7	0.6	ML	1
85	449715	AFAD	2019-10-16 05:23:51	38.1833	28.8321	7	0.31	ML	1.3
86	449086	AFAD	2019-10-06 22:53:44	38.3253	28.3255	7	0.62	ML	0.9
87	449080	AFAD	2019-10-06 22:05:34	38.2953	28.3233	9.73	0.48	ML	1.5
88	449034	AFAD	2019-10-05 17:34:28	38.2668	28.0261	7	0.32	ML	1.5
89	448505	AFAD	2019-09-29 18:42:23	38.5813	27906	7.04	0.48	ML	1.2
90	448162	AFAD	2019-09-27 11:04:50	38.4803	28.438	6.05	0.12	ML	1.4
91	447355	AFAD	2019-09-17 10:55:17	38.1231	28.4226	7	0.51	ML	1.4
92	446590	AFAD	2019-09-04 08:43:55	38.744	28287	6.99	0.26	ML	1.5
93	446037	AFAD	2019-08-27 09:48:40	38.274	28.7576	7	0.29	ML	2.9
94	444795	AFAD	2019-08-09 13:51:20	38.115	28.1706	7	0.39	ML	1
95	444609	AFAD	2019-08-08 12:13:31	38.1528	28849	7.05	0.7	ML	1

Table A1 continues

96	444550	AFAD	2019-08-08 01:41:17	38.2696	28.3278	6.98	0.19	ML	1.2
97	444163	AFAD	2019-07-30 14:07:01	38.1645	28.8696	7	0.54	ML	1.4
98	443997	AFAD	2019-07-26 11:20:11	38.5118	28.5125	7.19	0.5	ML	1
99	443790	AFAD	2019-07-22 21:54:10	38.2186	28.7951	7	0.59	ML	1
100	443702	AFAD	2019-07-21 13:48:30	38.1796	28703	7	0.32	ML	1
101	443499	AFAD	2019-07-19 07:19:34	38.5761	27948	5.12	0.66	ML	1.8
102	443389	AFAD	2019-07-17 03:04:10	38.1985	28.7655	7	0.6	ML	0.9
103	443381	AFAD	2019-07-17 01:41:56	38.1816	28.7805	7	0.6	ML	1
104	443380	AFAD	2019-07-17 01:39:11	38.1865	28.7691	7	0.51	ML	1.1
105	442970	AFAD	2019-07-08 15:29:22	38.3028	28.1225	7	0.66	ML	1
106	442642	AFAD	2019-07-01 01:40:47	38.276	28.7003	8.21	0.54	ML	1.2
107	442347	AFAD	2019-06-23 11:45:26	38.2203	28.3321	10.64	0.58	ML	1.1
108	442340	AFAD	2019-06-23 10:05:23	38.2463	28.3293	8.95	0.37	ML	1.1
109	441796	AFAD	2019-06-11 14:34:46	38.6031	28.0715	7	0.5	ML	1.1
110	440987	AFAD	2019-05-27 05:57:20	38.265	28.6653	7	0.18	ML	1
111	440618	AFAD	2019-05-21 02:01:40	38.3456	27.9258	7	0.67	ML	0.8
112	440518	AFAD	2019-05-18 17:37:59	38.085	28.2156	7	0.46	ML	1.3
113	440087	AFAD	2019-05-11 16:46:35	38.1931	28.8668	7	0.41	ML	1.6
114	438746	AFAD	2019-05-04 12:43:56	38.631	27.9643	6.63	0.9	ML	2
115	437225	AFAD	2019-04-12 07:25:07	38.3023	28.41	11.96	0.39	ML	1.7
116	437016	AFAD	2019-04-09 13:04:03	38.3425	28.6148	7	0.19	ML	1.1
117	436942	AFAD	2019-04-08 12:03:30	38.84	28.6203	7	0.51	ML	1.1
118	436940	AFAD	2019-04-08 11:58:02	38.3016	28.3421	7	0.14	ML	1.1
119	435865	AFAD	2019-03-29 19:02:45	38.2405	28.6433	7	0.67	ML	1.5
120	433475	AFAD	2019-03-19 23:20:07	38.2116	28.8125	7	0.42	ML	0.9
121	433118	AFAD	2019-03-14 21:55:56	38.2766	28.3251	7.04	0.26	ML	1.5
122	433084	AFAD	2019-03-14 11:49:30	38.3661	28.9288	7	0.36	ML	1.1
123	432628	AFAD	2019-03-07 11:20:26	38.4075	28.677	7	0.44	ML	1.1
124	430831	AFAD	2019-02-09 22:37:29	38.4845	28.3016	7	0.2	ML	1
125	429789	AFAD	2019-01-23 13:56:45	38.3896	28.7066	6.78	0.4	ML	1.1
126	429621	AFAD	2019-01-20 21:14:06	38.4148	28.6055	9.76	0.33	ML	1.1
127	429486	AFAD	2019-01-19 09:48:08	38.4713	28.4715	6.09	0.34	ML	1.4
128	429277	AFAD	2019-01-16 01:32:25	38.178	28.8076	9.33	0.29	ML	1.7

Table A1 continues

129	428988	AFAD	2019-01-12 00:00:32	38.1841	28.8285	7	0.41	ML	1
130	428517	AFAD	2019-01-04 12:50:15	38.302	28.4106	6.87	0.18	ML	1
131	428206	AFAD	2018-12-29 11:33:18	38.1193	28.1318	7	0.32	ML	1.3
132	427641	AFAD	2018-12-20 16:25:17	38.2855	28.2766	7.11	0.45	ML	1.8
133	427637	AFAD	2018-12-20 14:31:19	38.1656	28.8355	7	0.44	ML	1.3
134	427636	AFAD	2018-12-20 14:29:00	38.1765	28.8143	11.57	0.32	ML	1.8
135	427586	AFAD	2018-12-19 17:05:05	38.1841	28.8211	7	0.29	ML	1.8
136	427267	AFAD	2018-12-14 05:39:06	38.2375	28.2746	9.22	0.37	ML	1.7
137	427188	AFAD	2018-12-13 04:43:17	38.26	28.276	7	0.29	ML	1.3
138	426915	AFAD	2018-12-09 00:06:18	38.6973	28.0451	8.53	0.61	ML	1
139	426268	AFAD	2018-11-30 08:52:59	38.2685	28.6255	7	0.29	ML	0.8
140	425637	AFAD	2018-11-21 13:06:58	38.4048	28.7053	6.93	0.28	ML	1.3
141	425632	AFAD	2018-11-21 11:25:36	38.3998	28.6586	5.28	0.33	ML	1.1
142	425425	AFAD	2018-11-17 19:09:08	38.311	28.1506	7	0.27	ML	1.6
143	424324	AFAD	2018-11-04 16:09:48	38.4118	28.5746	9.94	0.19	ML	1.4
144	424121	AFAD	2018-11-01 09:44:37	38.5253	28.4765	6.01	0.27	ML	0.9
145	422790	AFAD	2018-10-14 04:09:25	38.6435	28.0195	7.48	0.19	ML	1.3
146	422625	AFAD	2018-10-11 09:42:51	38.5088	28.5791	6.89	0.1	ML	1.3
147	422597	AFAD	2018-10-10 20:53:42	38.6788	28.0025	7	0.44	ML	1.8
148	422527	AFAD	2018-10-10 06:07:10	38.734	28.1468	7.21	0.52	ML	1.4
149	421966	AFAD	2018-10-02 12:10:41	38.0765	28.2001	7	0.14	ML	1.1
150	421341	AFAD	2018-09-22 09:56:37	38.3933	28.6615	7	0.2	ML	1
151	421344	AFAD	2018-09-22 09:49:57	38.3636	28.9746	7	0.44	ML	1
152	421213	AFAD	2018-09-20 10:57:19	38.1586	28.8375	7	0.32	ML	1.5
153	421042	AFAD	2018-09-18 09:44:06	38.38.83	28.7405	6.1	0.15	ML	1.2
154	421021	AFAD	2018-09-18 07:36:12	38.1695	28.8506	6.99	0.32	ML	1.5
155	420945	AFAD	2018-09-17 09:30:14	38.296	28943	7	0.43	ML	1
156	420884	AFAD	2018-09-16 17:11:59	38.769	28.7855	7	0.67	ML	1.4
157	420113	AFAD	2018-09-08 09:41:32	38.357	28.9246	7	0.3	ML	1
158	419768	AFAD	2018-09-03 16:24:30	38.1748	28.8803	7	0.47	ML	1.6
159	419407	AFAD	2018-08-28 10:52:14	38.0216	28.4593	7.01	0.45	ML	2.1
160	419408	AFAD	2018-08-28 10:50:58	38.0101	28.4638	7	0.46	ML	1.8
161	419404	AFAD	2018-08-28 09:31:23	38.3851	28965	7	0.18	ML	0.8

Table A1 continues

162	419313	AFAD	2018-08-26 23:16:33	38.7016	28.1096	4.59	0.33	ML	1.9
163	419115	AFAD	2018-08-23 03:16:56	38.6273	28914	7	0.54	ML	1
164	418515	AFAD	2018-08-12 15:57:21	38.213	28.8435	7	0.35	ML	1.6
165	418333	AFAD	2018-08-08 10:41:46	38.399	28.9233	7	0.38	ML	1
166	418322	AFAD	2018-08-08 07:22:28	38.2943	28.9565	7	0.18	ML	1
167	418284	AFAD	2018-08-07 13:03:24	38.4261	28.5953	10.36	0.4	ML	0.7
168	418141	AFAD	2018-08-05 05:05:50	38.444	27.9203	7.01	0.32	ML	1.9
169	418122	AFAD	2018-08-04 10:05:30	38.6211	27.9343	7	0.3	ML	1.5
170	418066	AFAD	2018-08-03 21:53:34	38.3581	28.3803	7	0.57	ML	1.2
171	418037	AFAD	2018-08-03 12:56:27	38.4585	28.3868	6.78	0.13	ML	1
172	418028	AFAD	2018-08-03 11:26:50	38.3295	28.6746	6.47	0.8	ML	0.9
173	417859	AFAD	2018-07-31 18:43:28	38.3655	28.9468	7	0.37	ML	1.7
174	417515	AFAD	2018-07-26 09:52:17	38.3403	28.9628	7	0.17	ML	0.8
175	417211	AFAD	2018-07-22 12:53:18	38.7121	28184	6.85	0.41	ML	1.3
176	416915	AFAD	2018-07-17 12:25:05	38.3958	28.7143	8.14	0.8	ML	1.1
177	416914	AFAD	2018-07-17 12:09:41	38.3501	28.9388	7	0.27	ML	0.9
178	416526	AFAD	2018-07-10 13:45:11	38.5701	27.9585	8.43	0.66	ML	0.7
179	416248	AFAD	2018-07-06 10:46:57	38.4736	28.441	7	0.4	ML	1.2
180	416076	AFAD	2018-07-03 16:46:19	38.5943	28.1751	7	0.37	ML	1.5
181	415802	AFAD	2018-06-27 11:25:30	38.4673	28.449	7	0.6	ML	1.3
182	415698	AFAD	2018-06-25 10:11:23	38.1583	28168	7	0.58	ML	0.9
183	415572	AFAD	2018-06-22 13:38:10	38.3378	28.7205	14.33	0.5	ML	0.8
184	414404	AFAD	2018-06-19 07:40:25	38.6253	28.6113	7	0.52	ML	1
185	413936	AFAD	2018-06-11 07:42:05	38.6411	28094	6.99	0.63	ML	1.7
186	413678	AFAD	2018-06-06 19:06:26	38.6198	27.9656	12.22	0.52	ML	2.3
187	413542	AFAD	2018-06-03 16:30:20	38.3813	28.655	7.22	0.39	ML	1.2
188	413403	AFAD	2018-05-31 11:30:14	38.395	28.7361	7	0.42	ML	1.1
189	413261	AFAD	2018-05-29 16:32:09	38.3726	28.6453	7	0.25	ML	1
190	413096	AFAD	2018-05-26 17:14:21	38.6953	28.0336	12.46	0.14	ML	1.6
191	412631	AFAD	2018-05-18 03:45:37	38.1618	28.8546	7	0.31	ML	1.6
192	412097	AFAD	2018-05-09 08:13:42	38.6325	28.5693	7	0.21	ML	1.1
193	411807	AFAD	2018-05-04 12:12:48	38.6568	28.5363	7	0.37	ML	1.4
194	411561	AFAD	2018-05-01 02:55:47	38.6343	27.9378	7	0.39	ML	1.5

Table A1 continues

195	410622	AFAD	2018-04-17 09:12:55	38.6	28.5855	7	0.33	ML	1.2
196	409935	AFAD	2018-04-06 13:37:04	38.4743	28.4956	9.44	0.12	ML	1
197	408918	AFAD	2018-03-20 22:47:44	38.6418	28.8768	7	0.51	ML	1
198	408394	AFAD	2018-03-14 03:33:29	38.8101	28.2015	7	0.39	ML	1.1
199	407499	AFAD	2018-03-01 17:06:03	38.2281	28.7001	7	0.56	ML	1.2
200	405679	AFAD	2018-02-26 01:31:54	38.108	28.4901	11.29	0.5	ML	1.5
201	403502	AFAD	2018-02-10 22:14:02	38.466	27.8936	6.98	0.37	ML	1.9
202	403432	AFAD	2018-02-09 21:26:19	38.6151	27.9651	7.39	0.51	ML	1.5
203	403358	AFAD	2018-02-08 23:04:42	38.2846	28.6583	7	0.29	ML	1.4
204	403097	AFAD	2018-02-05 14:34:17	38.3548	28.3986	7.02	0.42	ML	1.4
205	402680	AFAD	2018-01-30 15:34:13	38.201	28.8661	7	0.21	ML	1.4
206	402539	AFAD	2018-01-29 00:57:04	38.3506	28.396	7	0.5	ML	1.4
207	402159	AFAD	2018-01-23 09:04:39	38.1561	28.0566	7.73	0.66	ML	1.2
208	401502	AFAD	2018-01-15 13:11:09	38.5228	28.8826	7	0.92	ML	1.2
209	401497	AFAD	2018-01-15 11:07:30	38.3585	28.3986	7	0.38	ML	1.7
210	401469	AFAD	2018-01-14 23:36:01	38.7343	28.4688	7.06	0.87	ML	1.5
211	401442	AFAD	2018-01-14 17:02:51	38.7135	28.0373	7.3	0.2	ML	1.7
212	401169	AFAD	2018-01-11 09:23:54	38.0538	28.49	7	0.25	ML	1.2
213	400916	AFAD	2018-01-09 00:27:24	38.3176	27.9236	7	0.26	ML	1
214	400775	AFAD	2018-01-07 09:06:04	38.3395	28.4128	7	0.43	ML	3.4
215	400493	AFAD	2018-01-04 19:20:57	38.3623	28.4225	7	0.19	ML	1
216	400300	AFAD	2018-01-02 05:12:18	38.3133	28.5155	7	0.35	ML	0.9
217	400299	AFAD	2018-01-02 05:09:54	38.3208	28.5205	7	0.32	ML	1.1
218	400156	AFAD	2017-12-31 08:37:10	38.3448	28.4315	7	0.34	ML	1.2
219	399962	AFAD	2017-12-29 01:03:58	38.7473	28.7593	6.8	0.39	ML	1.3
220	399812	AFAD	2017-12-27 10:36:26	38.5606	27.9635	7	0.45	ML	1.4
221	399742	AFAD	2017-12-26 20:14:14	38.6448	27.9321	7	0.3	ML	1.3
222	399508	AFAD	2017-12-25 00:46:30	38.1813	28.8688	7	0.47	ML	1
223	399391	AFAD	2017-12-23 22:38:25	38.3715	28.3803	7	0.46	ML	1.1
224	399377	AFAD	2017-12-23 19:10:35	38.3656	28.3623	7	0.33	ML	2
225	399333	AFAD	2017-12-23 02:39:42	38.3551	28.3598	7.01	0.38	ML	1.5
226	399051	AFAD	2017-12-19 11:01:00	38.3535	28.4075	7	0.35	ML	1
227	398973	AFAD	2017-12-18 17:42:59	38.3648	28.4125	7	0.5	ML	1.3

Table A1 continues

228	398772	AFAD	2017-12-15 23:38:16	38.1468	28.7728	6.82	0.14	ML	1
229	398733	AFAD	2017-12-15 09:37:30	38.3491	28.4078	7.02	0.28	ML	1.7
230	398724	AFAD	2017-12-15 08:36:21	38.3521	28.4276	10.86	0.51	ML	2.2
231	398722	AFAD	2017-12-15 07:31:44	38.359	28.4293	10.88	0.52	ML	2.4
232	398664	AFAD	2017-12-14 17:04:10	38.3738	28398	7	0.16	ML	1.1
233	398282	AFAD	2017-12-09 16:56:49	38.3496	28.3813	7	0.42	ML	1.4
234	398265	AFAD	2017-12-09 11:22:37	38.5401	28.6483	6.91	0.5	ML	1.1
235	398188	AFAD	2017-12-08 14:05:36	38.364	28.3908	7	0.52	ML	1.7
236	398033	AFAD	2017-12-06 17:56:03	38.3805	28.1025	6.91	0.55	ML	1.9
237	397963	AFAD	2017-12-05 22:54:55	38.3688	28.3491	7	0.71	ML	1
238	397837	AFAD	2017-12-04 06:44:19	38.3931	28.3646	7	0.25	ML	1.3
239	397794	AFAD	2017-12-03 11:38:22	38.4195	28.4018	7	0.46	ML	1.3
240	397756	AFAD	2017-12-03 01:37:09	38.3591	28.3903	7	0.4	ML	1.3
241	397727	AFAD	2017-12-02 13:45:13	38.424	28.0276	7	0.78	ML	1.2
242	397669	AFAD	2017-12-02 01:35:21	38.392	28.4226	7	0.49	ML	1.3
243	397668	AFAD	2017-12-02 01:28:30	38.3676	28405	7.13	0.4	ML	1.7
244	397667	AFAD	2017-12-02 01:17:14	38.3925	28.4198	7	0.28	ML	1.1
245	397666	AFAD	2017-12-02 01:14:46	38.359	28.4016	7.07	0.46	ML	2.8
246	397664	AFAD	2017-12-02 01:07:20	38.3705	28.3768	7	0.56	ML	1.2
247	397469	AFAD	2017-11-29 06:06:02	38.4298	28.4505	7	0.18	ML	1.3
248	397421	AFAD	2017-11-28 21:14:09	38.4071	28.3981	7	0.74	ML	1.1
249	397184	AFAD	2017-11-26 02:56:25	38.3521	28.4238	6.26	0.37	ML	1.4
250	397088	AFAD	2017-11-25 13:26:00	38.3668	28.3803	7	0.18	ML	1.8
251	396771	AFAD	2017-11-23 03:04:53	38.7008	28.2655	7.22	0.87	ML	1.3
252	396470	AFAD	2017-11-20 01:49:48	38.4076	28.5396	9.66	0.32	ML	1.1
253	396469	AFAD	2017-11-20 01:40:47	38.444	28.5211	10.83	0.23	ML	1
254	396468	AFAD	2017-11-20 01:40:19	38.4086	28.5698	7.57	0.35	ML	1.5
255	396272	AFAD	2017-11-17 21:31:10	38.6996	28.1215	8.54	0.39	ML	1.1
256	395947	AFAD	2017-11-14 16:39:37	38.6116	28.0511	5.46	0.5	ML	1.2
257	395432	AFAD	2017-11-08 23:35:03	38.6083	27.9985	8.28	0.21	ML	1.4
258	395127	AFAD	2017-11-06 03:03:00	38.1995	28.8828	7	0.51	ML	1
259	395063	AFAD	2017-11-05 03:24:13	38.3421	28.3936	7	0.44	ML	1
260	395062	AFAD	2017-11-05 03:01:27	38.3588	28.4161	7	0.28	ML	1

Table A1 continues

261	395031	AFAD	2017-11-04 19:17:34	38.4663	28.1606	7	0.38	ML	1.2
262	394807	AFAD	2017-11-02 05:59:26	38.4928	28.5103	25.1	0.84	ML	1.3
263	394806	AFAD	2017-11-02 05:45:33	38.5008	28.5026	20.4	0.36	ML	1
264	394804	AFAD	2017-11-02 05:03:40	38.3751	28375	7	0.34	ML	1.4
265	394526	AFAD	2017-10-29 23:40:33	38.3436	28.5845	7	0.41	ML	1.4
266	394272	AFAD	2017-10-26 21:01:49	38.495	27.9598	7	0.44	ML	1
267	393865	AFAD	2017-10-22 00:41:00	38.7003	28.09	8.57	0.12	ML	0.9
268	393690	AFAD	2017-10-20 10:59:15	38.383	28.6868	6.86	0.15	ML	1.4
269	393628	AFAD	2017-10-19 19:48:17	38.3848	28.4158	7	0.6	ML	1.8
270	393559	AFAD	2017-10-19 03:03:01	38.7005	27.9873	10.91	0.57	ML	1.1
271	393023	AFAD	2017-10-13 03:27:30	38.656	27.9346	10.84	0.39	ML	1.4
272	392947	AFAD	2017-10-12 14:13:29	38.4701	28.5115	6.76	0.3	ML	1.2
273	392638	AFAD	2017-10-09 04:30:03	38.432	28.5333	6.59	0.1	ML	1.2
274	392300	AFAD	2017-10-06 00:56:08	38.579	27.9071	7	0.49	ML	1.6
275	392196	AFAD	2017-10-05 05:14:17	38.7503	28084	6.67	0.41	ML	1.2
276	392194	AFAD	2017-10-05 04:57:35	38.7213	28.0268	11.06	0.35	ML	1.9
277	392192	AFAD	2017-10-05 04:03:26	38.7465	28.0916	7.41	0.26	ML	1.2
278	392191	AFAD	2017-10-05 04:01:05	38.722	28.0753	6.49	0.45	ML	1.1
279	392188	AFAD	2017-10-05 03:57:28	38.7313	27.9913	12.38	0.58	ML	1.6
280	392183	AFAD	2017-10-05 02:12:04	38.675	28.0116	10.46	0.26	ML	1
281	392182	AFAD	2017-10-05 02:10:54	38.6573	28.0373	15.63	0.6	ML	1.2
282	392166	AFAD	2017-10-04 22:00:44	38.6398	27.99	15.47	0.7	ML	1
283	392165	AFAD	2017-10-04 21:47:50	38.6885	28.0351	13.24	0.36	ML	1.1
284	392160	AFAD	2017-10-04 20:47:58	38.727	28.0731	6.85	0.45	ML	1.1
285	392159	AFAD	2017-10-04 20:36:00	38.7005	28.0288	11.09	0.39	ML	1.4
286	392158	AFAD	2017-10-04 20:32:19	38.6836	28.0873	8.39	0.67	ML	1.2
287	392152	AFAD	2017-10-04 19:29:04	38.719	28.1013	5.91	0.32	ML	1.4
288	392150	AFAD	2017-10-04 19:01:53	38.6528	27.9628	9.51	0.71	ML	1.3
289	392149	AFAD	2017-10-04 18:39:12	38.6823	28.0758	8.74	0.1	ML	1.2
290	392141	AFAD	2017-10-04 17:52:20	38.6595	27.9436	7.74	0.38	ML	1.4
291	392139	AFAD	2017-10-04 17:30:04	38.7496	28.0828	6.75	0.49	ML	1.5
292	392137	AFAD	2017-10-04 17:19:37	38.6636	27.9948	11.38	0.43	ML	1.3
293	392078	AFAD	2017-10-03 18:53:22	38.1141	28.8018	16.36	0.16	ML	1.2

Table A1 continues

294	392022	AFAD	2017-10-03 00:02:50	38.4996	28.5058	20.02	0.5	ML	1
295	391833	AFAD	2017-09-30 09:49:33	38.3471	27.9823	7	0.16	ML	1.5
296	391668	AFAD	2017-09-27 23:52:35	38.0685	28.3778	7	0.19	ML	1.7
297	391635	AFAD	2017-09-27 10:20:46	38.387	28702	3.1	0	ML	1.2
298	391339	AFAD	2017-09-23 11:42:26	38.4643	28.4598	4.2	0.5	ML	1.2
299	391279	AFAD	2017-09-22 20:01:47	38.4495	28.6051	7.76	0.22	ML	1.2
300	391278	AFAD	2017-09-22 19:57:10	38.4775	28566	10.29	0.65	ML	1.1
301	391277	AFAD	2017-09-22 19:55:40	38.4478	28.5498	11.53	0.43	ML	1.2
302	391276	AFAD	2017-09-22 19:54:35	38.4353	28.5801	9.09	0.47	ML	1.4
303	391275	AFAD	2017-09-22 19:52:44	38.4266	28.5735	9.19	0.5	ML	1.4
304	390955	AFAD	2017-09-18 20:48:39	38.5551	28.9663	7	0.53	ML	1.1
305	390502	AFAD	2017-09-13 19:47:30	38.3901	28.4158	7	0.35	ML	1.4
306	390448	AFAD	2017-09-13 07:47:06	38.1343	28589	7	0.16	ML	1.5
307	390258	AFAD	2017-09-11 05:09:12	38.38	28414	7	0.25	ML	1.5
308	389823	AFAD	2017-09-07 00:34:26	38.373	28.5146	6.7	0.53	ML	1
309	389742	AFAD	2017-09-06 06:13:25	38.666	28.1221	7	0.2	ML	1
310	389228	AFAD	2017-09-01 07:22:25	38.4543	27.9908	7	0.24	ML	1.3
311	389163	AFAD	2017-08-31 21:03:09	38.5531	28.9755	7.02	0.51	ML	1.4
312	388838	AFAD	2017-08-28 16:36:42	38.3441	28.0885	8.65	0.32	ML	1.6
313	388755	AFAD	2017-08-27 22:39:17	38.3548	28.4621	7	0.29	ML	1
314	388589	AFAD	2017-08-26 10:02:52	38.5161	28.4705	3.94	0.5	ML	1.5
315	388030	AFAD	2017-08-21 09:00:18	38.5661	28.8558	7	0.41	Md	1.7
316	387766	AFAD	2017-08-19 02:00:38	38.4563	27.9198	7	0.18	ML	1.5
317	387519	AFAD	2017-08-17 17:19:52	38.6528	28.0491	7.03	0.15	ML	1.1
318	387462	AFAD	2017-08-17 03:50:51	38.694	27.9861	6.98	0.64	ML	2.2
319	387461	AFAD	2017-08-17 02:49:49	38.4086	28.4011	7	0.16	ML	1.1
320	387436	AFAD	2017-08-16 17:12:21	38.3645	28.4678	7	0.1	ML	1
321	387405	AFAD	2017-08-16 11:18:34	38.5593	28.6315	7.21	0.11	ML	1.2
322	387321	AFAD	2017-08-15 23:54:18	38.5866	28.8955	7	0.44	ML	1.3
323	387150	AFAD	2017-08-14 18:32:20	38.7105	28.2008	7.01	0.52	ML	1.2
324	385602	AFAD	2017-08-07 17:56:28	38.3585	28.4161	7	0.47	ML	2.3
325	384973	AFAD	2017-08-04 13:15:14	38.6948	28.0243	11.12	0.18	ML	1.4
326	384969	AFAD	2017-08-04 13:14:14	38.6533	28.0126	3	0.79	ML	2.2

Table A1 continues

327	384968	AFAD	2017-08-04 13:13:56	38.6321	28.0156	5.46	0.26	ML	2.2
328	384422	AFAD	2017-08-01 05:43:18	38.4668	28.0836	7	0.16	ML	1.3
329	384373	AFAD	2017-07-31 23:46:27	38.3448	28.5201	7	0.53	ML	1.7
330	384258	AFAD	2017-07-31 14:49:11	38.6886	28078	7.22	0.6	ML	1
331	383223	AFAD	2017-07-26 05:22:14	38.6135	28.0236	6.22	0.46	ML	2.4
332	382690	AFAD	2017-07-24 02:37:33	38.7281	27.9941	7	0.14	ML	1
333	382475	AFAD	2017-07-23 06:07:42	38.3516	28439	7	0.33	ML	1.8
334	382428	AFAD	2017-07-23 03:06:49	38.3516	28.4036	7	0.19	ML	1.5
335	381373	AFAD	2017-07-19 16:26:23	38.3731	28424	7.59	0.36	ML	2.2
336	381374	AFAD	2017-07-19 16:24:18	38.3985	28.4376	7	0.45	ML	2
337	381137	AFAD	2017-07-16 14:53:01	38.3213	28.4371	7	0.71	ML	1.1
338	381133	AFAD	2017-07-16 13:47:39	38.3533	28425	7	0.45	ML	1.3
339	381131	AFAD	2017-07-16 13:07:46	38.2701	28.6948	5.55	0.26	ML	2.2
340	381129	AFAD	2017-07-16 12:50:45	38.283	28.7078	7.66	0.32	ML	1.8
341	381127	AFAD	2017-07-16 12:40:06	38.3371	28733	7.57	0.17	ML	1.2
342	380847	AFAD	2017-07-13 07:13:28	38.3583	28.4765	7	0.18	ML	1.1
343	380656	AFAD	2017-07-10 14:46:34	38.3926	28.5195	6.88	0.28	ML	1
344	380412	AFAD	2017-07-07 23:22:11	38.4133	28503	14.78	0.5	ML	1.5
345	380396	AFAD	2017-07-07 17:56:27	38.352	28.4256	7	0.28	ML	1.3
346	380385	AFAD	2017-07-07 15:49:52	38.3881	28.4771	7	0.17	ML	1
347	380113	AFAD	2017-07-03 23:16:21	38.3736	28.4276	7	0.48	ML	1.5
348	380033	AFAD	2017-07-03 07:15:22	38.3745	28.4636	7	0.15	ML	1
349	379964	AFAD	2017-07-02 13:49:35	38.3471	28.4076	7	0.55	ML	2
350	379963	AFAD	2017-07-02 13:47:51	38.3488	28.3928	7	0.44	ML	1.7
351	379826	AFAD	2017-07-01 02:08:38	38.5015	28506	17.47	0.43	ML	1
352	379797	AFAD	2017-06-30 21:50:34	38.3728	28.4555	7	0.28	ML	1
353	379794	AFAD	2017-06-30 21:39:26	38.3801	28518	6.12	0.44	ML	1
354	379782	AFAD	2017-06-30 18:24:27	38.2908	28539	7	0.4	ML	1
355	378837	AFAD	2017-06-30 05:31:27	38.3326	28.4316	7	0.32	ML	1.3
356	378823	AFAD	2017-06-30 02:17:44	38.3475	28.4558	7	0.23	ML	1.9
357	378811	AFAD	2017-06-30 00:36:25	38.3511	28.4338	7	0.3	ML	1.5
358	378773	AFAD	2017-06-29 15:56:49	38.35	28.39	7	0.32	ML	1.4
359	378703	AFAD	2017-06-29 01:58:16	38.3618	28.4326	7	0.4	ML	1.4

Table A1 continues

360	378691	AFAD	2017-06-29 00:01:23	38.3438	28.3388	7	0.31	ML	1.2
361	378593	AFAD	2017-06-28 01:31:48	38.3568	28.4326	7	0.28	ML	1.3
362	378562	AFAD	2017-06-27 22:10:54	38.4275	28.5833	6.28	0.3	ML	1.1
363	378440	AFAD	2017-06-27 01:02:03	38.4855	28.5386	16.32	0.29	ML	1.1
364	378399	AFAD	2017-06-26 19:40:55	38.3545	28411	7	0.46	ML	1.1
365	378394	AFAD	2017-06-26 19:16:22	38.3621	28.3961	7	0.41	ML	1.6
366	378390	AFAD	2017-06-26 18:56:13	38.3516	28.3933	7	0.17	ML	1.5
367	378388	AFAD	2017-06-26 18:36:05	38.3455	28.4011	7	0.26	ML	1.3
368	378342	AFAD	2017-06-26 09:24:18	38.3593	28.4771	7	0.5	ML	1
369	378331	AFAD	2017-06-26 07:47:50	38.3435	28.3316	7	0.53	ML	1
370	378305	AFAD	2017-06-26 03:21:45	38.3576	28.3868	7	0.69	ML	1.2
371	378181	AFAD	2017-06-24 21:44:31	38.3691	28.4945	7	0.23	ML	0.9
372	377336	AFAD	2017-06-19 04:13:44	38.3845	28.3783	7	0.16	ML	1.2
373	376866	AFAD	2017-06-17 11:28:20	38.4256	28.3643	7	0.46	ML	1.6
374	376557	AFAD	2017-06-15 20:17:41	38.5935	28.0561	10.23	0.51	ML	1.4
375	376543	AFAD	2017-06-15 17:15:20	38.3378	28.3863	7.64	0.66	ML	2.1
376	376507	AFAD	2017-06-15 12:32:27	38.3806	28698	6.53	0.22	ML	1
377	376036	AFAD	2017-06-13 15:49:27	38.3566	28.3931	7	0.4	ML	1.8
378	375507	AFAD	2017-06-11 19:40:47	38.3555	28.3915	7	0.25	ML	1.4
379	375432	AFAD	2017-06-10 19:10:23	38.7538.	28.0858	5.81	0.43	ML	1
380	375417	AFAD	2017-06-10 15:10:28	38.3636	28.4028	7	0.38	ML	1.6
381	375359	AFAD	2017-06-10 00:21:19	38.4076	28.4363	7	0.14	ML	1.1
382	375189	AFAD	2017-06-07 22:42:23	38.5588	28.4396	7	0.25	ML	1
383	375162	AFAD	2017-06-07 18:52:53	38.573	28.8951	7	0.25	ML	1.1
384	375161	AFAD	2017-06-07 18:50:14	38.3493	28.4483	7	0.16	ML	1.3
385	375160	AFAD	2017-06-07 18:48:12	38.353	28.4773	7.02	0.47	ML	1.5
386	375095	AFAD	2017-06-07 05:40:29	38.2995	28.7345	8.72	0.5	ML	1.1
387	374637	AFAD	2017-06-02 15:33:02	38.2633	28276	7	0.26	ML	1.5
388	374621	AFAD	2017-06-02 11:25:50	38.3676	28.4376	7	0.21	ML	1.1
389	374541	AFAD	2017-06-01 21:55:34	38.2621	28.6581	7	0.22	ML	1.2
390	374274	AFAD	2017-05-31 04:39:56	38.361	28.4006	7.06	0.45	ML	1.8
391	373905	AFAD	2017-05-28 21:57:18	38.6176	27.9713	7	0.37	ML	1.2
392	373886	AFAD	2017-05-28 21:11:25	38.6923	28855	7	0.45	ML	1.2

Table A1 continues

393	373487	AFAD	2017-05-27 17:18:27	38.6201	27931	1.33	0.75	ML	1.8
394	373445	AFAD	2017-05-27 15:18:43	38.3215	28.2288	8.67	0.83	ML	1.8
395	373161	AFAD	2017-05-24 23:51:29	38.1065	28.5188	6.99	0.24	ML	1.6
396	373155	AFAD	2017-05-24 21:19:28	38.116	28.5181	7	0.31	ML	1.5
397	373088	AFAD	2017-05-23 17:55:11	38.7808	28285	7.04	0.23	ML	1.8
398	372947	AFAD	2017-05-22 00:17:01	38.3996	28015	7	0.37	ML	1.2
399	372868	AFAD	2017-05-20 20:48:12	38.3581	28.4011	7	0.33	ML	1.5
400	372844	AFAD	2017-05-20 11:42:16	38.3625	28.3865	7.4	0.38	ML	1.8
401	372837	AFAD	2017-05-20 10:36:39	38.3525	28.4018	7.11	0.29	ML	1.7
402	372833	AFAD	2017-05-20 10:27:02	38.37	28411	10.79	0.45	ML	2.6
403	372830	AFAD	2017-05-20 09:55:22	38.3673	28.4345	12.57	0.68	ML	1.6
404	372829	AFAD	2017-05-20 09:53:40	38.4063	28.4603	12.58	0.34	ML	2.2
405	372820	AFAD	2017-05-20 09:24:45	38.2766	28.3703	7	0.19	ML	1.3
406	372819	AFAD	2017-05-20 09:20:12	38.3641	28397	7	0.38	ML	1.5
407	372818	AFAD	2017-05-20 09:16:12	38.363	28386	7	0.26	ML	1.3
408	372814	AFAD	2017-05-20 09:05:50	38.3416	28.3738	7	0.34	ML	2
409	372811	AFAD	2017-05-20 08:53:08	38.3686	28399	7	0.36	ML	1.4

Appendix-2

Table A2 Well data of the study area

	WELL	WELL TYPE	DATE	DEPTH (m)	BOTTOM TEMP. (°C)	WELL HEAD TEMP. (°C)	FLOW (t/h)	X	Y	Z
1	GW-1	PRODUCTION	2012	3001	270	220	83	4249298	632768	154
2	GW-2	PRODUCTION	2013	3100	250	115	30	4249413	632162	155
3	GW-3	PRODUCTION	2013	2500	255	173	111	4248950	633840	153
4	GW-4	PRODUCTION	2012	3011	255	197	88	4249151	633129	156
5	GW-5	GRADIENT	2013	755	54	38	6	4241177	637254	173
6	GW-6	REINJECTION	2011	1566.00	172.00	90	225	4251716	625201	155
7	GW-7	GRADIENT	2011	2014.00	183.00	149	354	4251528	625718	160
8	GW-8	GRADIENT	2015	2462.00	168.00	92	251	4251729	626138	155
9	GW-9	PRODUCTION	2011	1512.00	200.00	178	300	4251084	623734	183
10	GW-10	PRODUCTION	2011	1604.00	197.00	174	280	4251588	623841	170
11	GW-11	PRODUCTION	2012	1059.00	202.00	185	315	4251480	623384	176
12	GW-12	OTHER	2012	1841.00	120.00	89	106	4244730	635917	175
13	GW-13	REINJECTION	2013	2391	170	80	30	4251150	628102	165
14	GW-14	REINJECTION	2015	1979	157	80	210	4251258	627538	160
15	GW-15	REINJECTION	2015	2210	162	80	45	4251285	627071	155
16	GW-16	GRADIENT	2012	1881	168	83	110	4245270	637022	170
17	GW-17	GRADIENT	2012	1011	-	-	-	4251308	623390	188
18	GW-18	REINJECTION	2014	1830	191	90	190	4251806	624774	152
19	GW-19	REINJECTION	2013	2718	174	90	150	4252208	625286	148
20	GW-20	PRODUCTION	2013	1359	188	167	180	4251890	623521	170
21	GW-21	PRODUCTION	2013	1560	194	175	315	4251768	623080	178
22	GW-22	OTHER	2013	2350	194	165	-	4252297	622588	173
23	GW-23	PRODUCTION	2013	2790	223	163	130	4252294	623902	145

Table A2 continues

24	GW-24	PRODUCTION	2014	1571	184	167	110	4252371	623439	151
25	GW-25	PRODUCTION	2015	1881	193	166	125	4252572	622959	155
26	GW-26	REINJECTION	2014	2727	208	90	165	4252853	624739	141
27	GW-27	REINJECTION	2014	2935	224	90	115	4253109	623759	141
28	GW-28	REINJECTION	2016	1841	170	80	115	4252250	624929	143
29	GW-29	REINJECTION	2016	2575	159	80	135	4251729	627637	146
30	GW-30	PRODUCTION	2017	3261	247	210	265	4248946	632741	156
31	GW-31	PRODUCTION	2017	3250	229	205	300	4248816	633206	155
32	GW-32	PRODUCTION	2017	3225	207	190	120	4248803	633202	152
33	GW-33	PRODUCTION	2017	2240	225	213	300	4248632	631924	166
34	GW-34	GRADIENT	2015	2133	-	-	-	4258280	614535	115
35	GW-35	REINJECTION	2016	2572	159	80	135	4251258	627550	150
36	GW-36	REINJECTION	2015	1841	170	145	310	4252250	624929	130
37	GW-37	REINJECTION	2014	2420	202	90	205	4253425	623140	141
38	GW-38	PRODUCTION	2013	1666	194	180	290	4251706	623080	178
39	GW-39	PRODUCTION	2015	1516	191	180	260	4252572	622959	155
40	GW-40	REINJECTION	2017	2823	222	94	50	4247962	632860	166
41	GW-41	REINJECTION	2017	3248	228	94	220	4247963	632854	166
42	GW-42	REINJECTION	2017	3402	202	94	65	4247951	632882	166
43	GW-43	REINJECTION	2017	3497	206	94	150	4247651	634205	156
44	GW-44	REINJECTION	2017	3244	225	94	415	4248939	632752	156
45	GW-45	PRODUCTION	2011	2752	238	236	100	4261735	607783	98
46	GW-46	PRODUCTION	2012	2747	232	232	1	4259974	606389	100
47	GW-47	GRADIENT	2012	480	32	29	36	4247903	639210	165
48	GW-48	PRODUCTION	2015	3589	140	138	64	4252167	630716	134
49	GW-49	PRODUCTION	2016	3112	150	149	120	4252595	630205	134
50	GW-50	PRODUCTION	2016	2968	155	155	410	4252186	631070	135

Table A2 continues

51	GW-51	PRODUCTION	2017	2863	151	95	200	4252003	631044	135
52	GW-52	PRODUCTION	2017	2407	155	-	-	4253365	630847	134
53	GW-53	GRADIENT	2012	480	42	41	65	4252280	630700	135
54	GW-54	GRADIENT	2012	400	32	31	10	4242937	642677	167
55	GW-55	GRADIENT	2012	530	51	50	60	4244580	641270	161
56	GW-56	PRODUCTION	2011	2301	167	165	298.8	4255228	623890	155
57	GW-57	PRODUCTION	2011	3100	230	230	3.6	4264430	602433	90
58	GW-58	PRODUCTION	2015	2894	209	145	247	4255250	623279	125
59	GW-59	PRODUCTION	2015	3041	195	180	261	4255051	623237	121
60	GW-60	PRODUCTION	2015	1631	128	122	600	4255032	624580	120
61	GW-61	PRODUCTION	2015	2042	169	124	700	4255032	625195	120
62	GW-62	REINJECTION	2015	1529	140	118	208	4255029	626301	122
63	GW-63	PRODUCTION	2015	1790	175	145	400	4255489	623430	120
64	GW-64	PRODUCTION	2015	1920	160	138	313	4255193	624125	121
65	GW-65	REINJECTION	2016	3325	164	145	234	4255369	623677	120
66	GW-66	REINJECTION	2015	984	140	135	32	4255123	626694	121
67	GW-67	REINJECTION	2016	1170	102	98	7	4256145	623861	123
68	GW-68	REINJECTION	2015	1238	111	108	148	4256427	623782	122
69	GW-69	PRODUCTION	2016	3430	159	128	151	4255191	624900	125
70	GW-70	REINJECTION	2016	1285	-	-	-	4255201	625982	126
71	GW-71	REINJECTION	2016	1300	-	-	-	4256243	623662	124
72	GW-72	PRODUCTION	2017	2800	162	149	82	4255194	624973	125
73	GW-73	PRODUCTION	2017	2200	166	153	98	4255174	624867	125
74	GW-74	PRODUCTION	2017	3100	171	162	-	4255220	625340	124
75	GW-75	EXLPORATION	1996	750.00	116.00	63	10	4253716	617807	150
76	GW-76	PRODUCTION	2011	2750.00	287.50	287	108	4256955	614408	120
77	GW-77	EXLPORATION	2011	1750.00	161.00	159.53	9	4249014	618936	326

Table A2 continues

78	GW-78	PRODUCTION	2011	2250.00	189.00	188	324	4255950	621000	126
79	GW-79	PRODUCTION	2002	1447.10	182.00	182	40	4255707	614902	172
80	GW-80	EXLPORATION	2004	1507.00	213.00	213.43	28	4252004	619490	216
81	GW-81	PRODUCTION	2012	2941	256	137	300	4255500	622000	125
82	GW-82	PRODUCTION	2012	3150	248	251	7	4256649	620001	130
83	GW-83	PRODUCTION	2013	3450	251	250	93	4254100	620500	140
84	GW-84	PRODUCTION	2013	3000	239	236	158	4255502	621289	139
85	GW-85	REINJECTION	2013	2750	214	214	36	4256385	621375	139
86	GW-86	PRODUCTION	2017	3176	220	219	201	4256399	621385	121
87	GW-87	PRODUCTION	2017	3000	230	220	327	4255544	621961	121
88	GW-88	PRODUCTION	2017	2808	224	224	306	4253978	622616	131
89	GW-89	PRODUCTION	2017	2736	213	210	590	4253973	622625	131
90	GW-90	PRODUCTION	2017	2660	215	214	453	4253967	622633	132
91	GW-91	REINJECTION	2018	2350	209	209	375	4253078	621521	160
92	GW-92	REINJECTION	2018	2595	217	217	333	4253082	621512	160
93	GW-93	REINJECTION	2018	2902	227	227	320	4253086	621502	160
94	GW-94	PRODUCTION	2018	2420	224	224	513	4253686	621464	149
95	GW-95	PRODUCTION	2018	3668	278	278	344	4253677	621459	149
96	GW-96	REINJECTION	2018	2102	203	203	493	4252656	621959	171
97	GW-97	PRODUCTION	2011	2946	186	161	258	4252565	629820	135
98	GW-98	PRODUCTION	2012	2672	187	161	321	4252947	628876	132
99	GW-99	REINJECTION	2017	2594	177	150	100	4253600	627993	136
100	GW-100	PRODUCTION	2017	3000	195	160	456	4252769	629353	134
101	GW-101	PRODUCTION	2017	1040	203	200	200	4251059	623143	220
102	GW-102	GRADIENT	2017	2124	137	-	-	4255463	629473	133
103	GW-103	PRODUCTION	2012	2515	171	150	198	4255324	624076	125
104	GW-104	REINJECTION	2011	3146	263	199	50	4258224	618072	120

Table A2 continues

105	GW-105	GRADIENT	2012	460	40	37	-	4266500	613512	203
106	GW-106	OTHER	2017	2400	-	-	-	4254305	629336	135
107	GW-107	PRODUCTION	2018	3433	211	160	70	4253277	628312	140
108	GW-108	REINJECTION	2017	2197	156	138	150	4253639	628000	136
109	GW-109	REINJECTION	2017	1870	143	139	300	4253639	628002	136
110	GW-110	PRODUCTION	2017	1380	203	200	370	4251438	622753	211
111	GW-111	GRADIENT	2017	1420	200	-	-	4250573	623657	227
112	GW-112	PRODUCTION	2017	1725	200	-	370	4251680	622436	233
113	GW-113	PRODUCTION	2017	1295	202	192	320	4251677	622426	233
114	GW-114	PRODUCTION	2017	2264	204	198	135	4251438	622763	203
115	GW-115	PRODUCTION	2018	1000	214	212	155	4250122	621947	340
116	GW-116	PRODUCTION	2017	1240	212	210	400	4249931	622751	295
117	GW-117	PRODUCTION	2017	915	202	202	270	4249740	623347	279
118	GW-118	PRODUCTION	2018	1400	202	200	225	4250310	622575	305
119	GW-119	REINJECTION	2018	1318	201	90	660	4248895	622738	386
120	GW-120	REINJECTION	2018	1161	165	90	300	4248448	622698	437
121	GW-121	REINJECTION	2018	2021	188	90	440	4248943	622292	517
122	GW-122	REINJECTION	2018	1054	195	90	640	4248906	622737	415
123	GW-123	REINJECTION	2018	1048	201	90	360	4249331	621776	500
124	GW-124	GRADIENT	2011	976	50	46	6	4244473	644640	170
125	GW-125	GRADIENT	2011	1033	60	59	4	4236620	642457	175
126	GW-126	GRADIENT	2015	2533	100	98	102	4241227	642497	172
127	GW-127	GRADIENT	2015	511	52	-	-	4254630	609450	336
128	GW-128	GRADIENT	2015	436	35	-	-	4246704	618323	626
129	GW-129	PRODUCTION	2015	1198.00	193.00	188.32	597.6	4250739	624870	167.00
130	GW-130	PRODUCTION	2011	1701.00	192.00	188.80	349.2	4251152	624924	162.00

Table A2 continues

131	GW-131	PRODUCTION	1995	1217.00	199.00	190.00	478	4251220	624292	163.00
132	GW-132	PRODUCTION	2012	920.00	203.00	197.00	518	4250136	624409	184.00
133	GW-133	PRODUCTION	2013	1255.00	188.00	168.00	144	4250430	625234	174.00
134	GW-134	PRODUCTION	2013	1132.00	197.00	189.00	378	4250789	624024	178.00
135	GW-135	REINJECTION	2013	1923.00	179.00	159.00	316	4251047	626245	165.00
136	GW-136	PRODUCTION	2015	1561	196	181.00	149	4250540	624430	179.00
137	GW-137	PRODUCTION	2015	1131	194	179.00	429	4250509	624440	174.00
138	GW-138	REINJECTION	2013	1857.00	174.00	120.00	126	4249897	626548	187.00
139	GW-139	REINJECTION	2013	1943.00	170.00	157.00	137	4249494	626799	212.00
140	GW-140	GRADIENT	2013	2253.00	-	-	-	4249335	627415	210.00
141	GW-141	REINJECTION	2013	1560.00	170.00	164.00	137	4250418	626340	182.00
142	GW-142	REINJECTION	2016	1554.00	174.00	100	180	4249928	626571	192.00
143	GW-143	REINJECTION	2014	1791	170	162	496	4250891	626815	165
144	GW-144	REINJECTION	2014	1360	172	160	496	4250243	625835	177
145	GW-145	REINJECTION	2014	1122	164	150	100	4248873	625249	124
146	GW-146	PRODUCTION	2015	3420	206	170	300	4250655	635083	143
147	GW-147	GRADIENT	2015	3634	205	-	-	4250610	635569	143
148	GW-148	PRODUCTION	2014	3150	211	208	156	4247335	623263	455
149	GW-149	PRODUCTION	2014	1750	172	178	210	4247740	622763	284
150	GW-150	PRODUCTION	2014	2194	184	140	280	4247382	622744	400
151	GW-151	PRODUCTION	2014	2438	200	144	200	4247635	623019	340
152	GW-152	PRODUCTION	2014	2970	229	229	150	4247928	622621	315
153	GW-153	REINJECTION	2015	3720	224	80	80	4246989	623123	570
154	GW-154	REINJECTION	2015	4064	219	80	77	4246575	623084	630
155	GW-155	REINJECTION	2015	3747	219	80	100	4247002	623089	570
156	GW-156	PRODUCTION	2016	2702	212	151	120	4247966	622564	315
157	GW-157	REINJECTION	2016	4312	238	-	-	4247966	622564	563

Table A2 continues

158	GW-158	PRODUCTION	2016	3184	227	80	100	4247396	622748	400
159	GW-159	PRODUCTION	2017	3880	224	140	130	4246903	622477	507
160	GW-160	REINJECTION	2016	2969	219	70	34	4247163	622809	468
161	GW-161	REINJECTION	2017	3831	217	150	220	4250103	635176	142
162	GW-162	PRODUCTION	2017	3616	245	170	160	4250699	634394	142
163	GW-163	PRODUCTION	2017	3945	215	177	350	4250648	634486	142
164	GW-164	REINJECTION	2019	3661	208	160	270	4250954	634097	141
165	GW-165	REINJECTION	2019	4284	208	100	120	4250932	634141	141
166	GW-166	REINJECTION	2012	1824	175	165	33	4247339	622894	359
167	GW-167	REINJECTION	2013	3355	206	155	150	4250347	634744	143
168	GW-168	OTHER	2012	3619	214	200	-	4249316	637193	146
169	GW-169	OTHER	1998	2120	141	-	-	4250980	634550	138
170	GW-170	OTHER	2001	2524	205	-	-	4248663	634308	145
171	GW-171	OTHER	2000	2450	157	-	-	4248421	633687	156
172	GW-172	OTHER	-	2120	-	-	-	4248434	633700	150
173	GW-173	GRADIENT	2013	2700	124	98	1	4248470	641985	179
174	GW-174	PRODUCTION	2017	906	199	178	97	4249723	624238	189
175	GW-175	REINJECTION	2017	2015	-	-	-	4250747	627049	165
176	GW-176	GRADIENT	2015	2145	172	-	-	4247725	629545	211
177	GW-177	OTHER	2016	2386	177	-	217	4248300	628539	227
178	GW-178	OTHER	2017	2400	174	-	-	4247937	629102	211
179	GW-179	OTHER	2017	2045	154	-	-	4247946	629097	211
180	GW-180	OTHER	2017	2683	195	-	194	4247827	627831	274
181	GW-181	OTHER	2017	2417	178	-	57	4247884	627853	274
182	GW-182	OTHER	2017	1824	147	-	133	4247717	628627	245
183	GW-183	OTHER	2017	3250	215	-	50	4248733	628633	200
184	GW-184	OTHER	2017	2058	152	-	-	4249734	629514	162

Table A2 continues

185	GW-185	PRODUCTION	2018	1090	198	-	299	4249053	624005	206
186	GW-186	PRODUCTION	2018	2725	226	172	47	4250124	623913	215
187	GW-187	PRODUCTION	2018	1039	200	178	288	4250114	623900	215
188	GW-188	OTHER	2018	2677	-	-	-	4249571	629477	162
189	GW-189	OTHER	2018	2595	175	-	-	4249764	628790	165
190	GW-190	OTHER	2018	2300	164	-	-	4249773	628784	165
191	GW-191	GRADIENT	2012	1764	185	78	-	4264133	609954	104
192	GW-192	GRADIENT	2012	3210	233	-	-	4263890	609911	104
193	GW-193	GRADIENT	2011	2750	95	-	-	4223900	648890	580
194	GW-194	GRADIENT	2017	680	34	29	1	4240091	637148	290
195	GW-195	GRADIENT	2018	2800	201	-	-	4255627	609028	187
196	GW-196	GRADIENT	2019	2800	140	-	-	4260300	624917	319
197	GW-197	GRADIENT	2020	2862	-	-	-	4248517	632576	162